Chapter 2

Cirrus Clouds

ANDREW J. HEYMSFIELD,[a] MARTINA KRÄMER,[b] ANNA LUEBKE,[b] PHIL BROWN,[c] DANIEL J. CZICZO,[d] CHARMAINE FRANKLIN,[e,k] PAUL LAWSON,[f] ULRIKE LOHMANN,[g] GREG MCFARQUHAR,[h] ZBIGNIEW ULANOWSKI,[i] AND KRISTOF VAN TRICHT[j]

[a] *National Center for Atmospheric Research, Boulder, Colorado*
[b] *Forschungszentrum Jülich GmbH, Jülich, Germany*
[c] *Met Office, Exeter, United Kingdom*
[d] *Massachusetts Institute of Technology, Cambridge, Massachusetts*
[e] *CSIRO Oceans and Atmosphere, Aspendale, Victoria, Australia*
[f] *SPEC Inc., Boulder, Colorado*
[g] *ETH, Zurich, Switzerland*
[h] *University of Illinois at Urbana–Champaign, Urbana, Illinois*
[i] *University of Hertfordshire, Hatfield, United Kingdom*
[j] *Katholieke Universiteit Leuven, Leuven, Belgium*

ABSTRACT

The goal of this chapter is to synthesize information about what is now known about one of the three main types of clouds, cirrus, and to identify areas where more knowledge is needed. Cirrus clouds, composed of ice particles, form in the upper troposphere, where temperatures are generally below $-30°C$. Satellite observations show that the maximum-occurrence frequency of cirrus is near the tropics, with a large latitudinal movement seasonally. In situ measurements obtained over a wide range of cirrus types, formation mechanisms, temperatures, and geographical locations indicate that the ice water content and particle size generally decrease with decreasing temperature, whereas the ice particle concentration is nearly constant or increases slightly with decreasing temperature. High ice concentrations, sometimes observed in strong updrafts, result from homogeneous nucleation. The satellite-based and in situ measurements indicate that cirrus ice crystals typically differ from the simple, idealized geometry for smooth hexagonal shapes, indicating complexity and/or surface roughness. Their shapes significantly impact cirrus radiative properties and feedbacks to climate. Cirrus clouds, one of the most uncertain components of general circulation models (GCM), pose one of the greatest challenges in predicting the rate and geographical pattern of climate change. Improved measurements of the properties and size distributions and surface structure of small ice crystals (about $20 \mu m$) and identifying the dominant ice nucleation process (heterogeneous versus homogeneous ice nucleation) under different cloud dynamical forcings will lead to a better representation of their properties in GCM and in modeling their current and future effects on climate.

1. Introduction

There are 10 basic cloud types, grouped into three primary categories: high clouds, mid clouds, and low clouds (http://www.srh.noaa.gov/srh/jetstream/clouds/cloudwise/types.html). The focus of this study is to characterize the macrophysical and microphysical properties of the high clouds: cirrus. The motivation for this chapter comes from workshops conducted on "Data Analysis and Presentation of Cloud Microphysical Measurements" in Seaside, Oregon, in 2010, at the Swiss Federal Institute of Technology (ETH) in Zurich in 2013, and at the Massachusetts Institute of Technology (MIT) in 2014. There was a clear need identified at the workshop and in discussions that followed to provide a synthesis of the current understanding of cirrus.

The focus of this chapter is to use observations of, and measurements within, cirrus clouds to characterize their

[k] Current affiliation: Bureau of Meteorology, Docklands, Victoria, Australia.

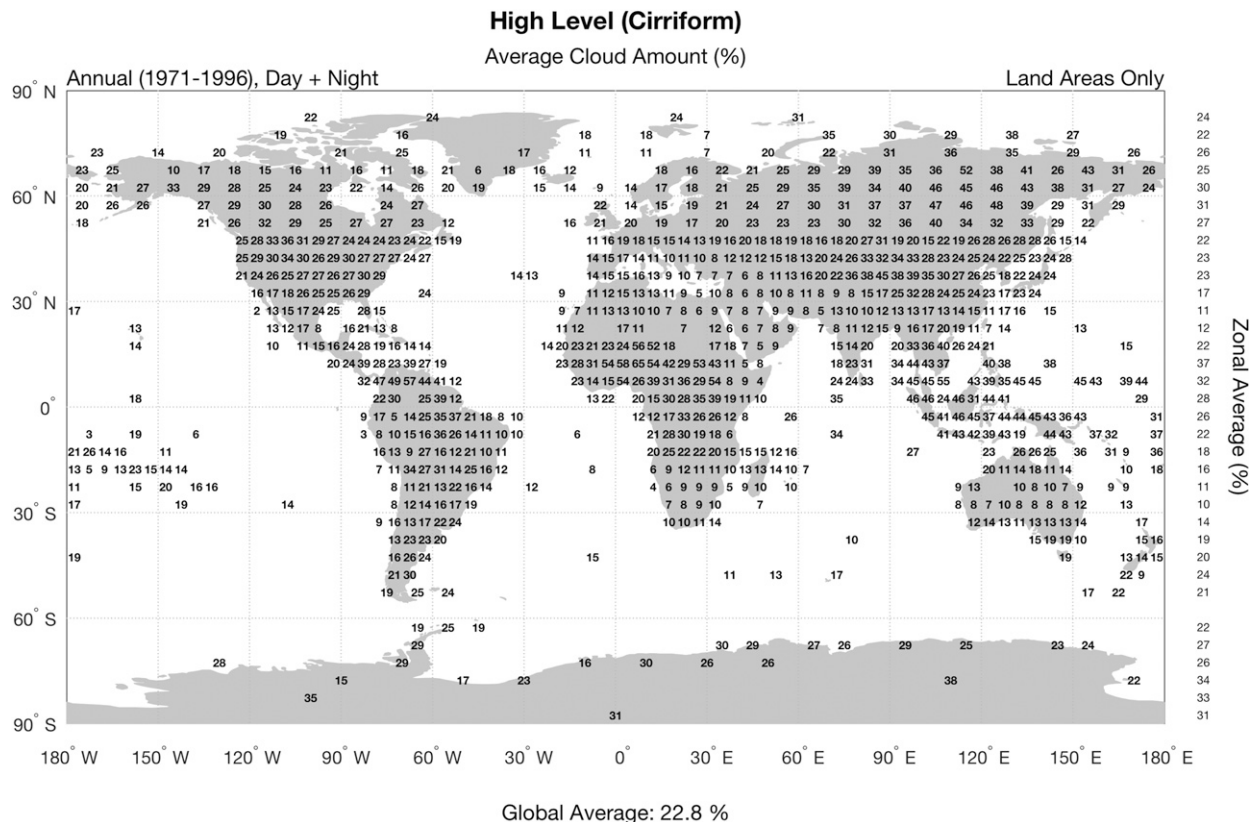*Corresponding author e-mail*: Andrew Heymsfield, heyms1@ucar.edu

FIG. 2-1. Fractional cirrus cloud coverage as obtained from a large database of observations collected at the ground and from ships over the period of 1971–96 (see text). Figure kindly prepared by Ryan Eastman, University of Washington.

properties. We describe the macrophysical properties of cirrus, how they form, their microphysical properties, their radiative properties, and their feedbacks to climate. The chapter concludes with a summary of areas in need of further study.

2. General description of cirrus types and macroscale properties

The *Glossary of Meteorology* (Huschke 1970) defines cirrus clouds as detached clouds in the form of white, delicate filaments, or white or mostly white patches, that are composed of ice crystals. Cirrus clouds form primarily in the upper troposphere, above about 8 km (25 000 ft), where temperatures are generally below −30°C. From tropical to polar regions, the frequency of cirrus cloud occurrence decreases from about 33% to 7%, median cirrus cloud-top heights decrease from 14 to 8 km, cloud thickness decreases from 2.8 to 1.4 km, and cloud-top temperatures increases from about −73° to −60°C (Sassen et al. 2008, 2009; see Figs. 2-2–2-4, below). Cirrus clouds can be horizontally and vertically extensive, especially when they are the

result of ice mass outflow from thunderstorms. An excellent cirrus cloud coverage climatology has been derived from a large set of cloud observations collected over decades from observations at the ground and from ships (Hahn and Warren 2007; see Fig. 2-1). The statistics indicate that the coverage is about 30% over North America and Asia, of the same order over parts of Europe that are not blocked by lower cloud, is in the 15%–20% range over South America, and as high as 50% over equatorial regions of Africa, diminishing toward 10% in the southernmost regions of Africa and about 10% over Australia. In the polar regions of the Northern Hemisphere, averages are on the order of 20%–45% and in the Southern Hemisphere they are about 25%.

The primary cirrus cloud types are cirrus, cirrostratus, and cirrocumulus. Cirrus are fibrous, threadlike, white feather clouds of ice crystals that resembles hair curls in form. Details can be found in WMO (1956) and in American Meteorological Society (2012) but are summarized here. Cirrostratus, the most frequently occurring cirrus clouds, which are found in layers or sheets with horizontal dimensions of hundreds or even

thousands of kilometers, are a milky, translucent cloud veil of ice crystals, which sometimes cause the appearance of halos around the moon and sun. Cirrocumulus are fleecy clouds, with cloud banks of small, white flakes.

Each of the primary cirrus types have species associated with them. The category cirrus includes the subspecies uncinus, which form in a patchy or tufted shape when the ice crystals are large enough to acquire an appreciable fall velocity (the rate at which ice crystals fall in the vertical) so that trails of considerable vertical extent (fallstreaks) may form. These trails curve irregularly or slant, sometimes with a commalike shape, as a result of changes in the horizontal wind velocity with height and variations in the fall velocity of the ice crystals. Cirrostratus includes the species fibratus, which have fibrous veils. Cirrocumulus includes the species lenticularis, which are lens shaped or almond shaped, often long stretched bands with sharply minted outlines and are often associated with mountainous areas.

There are particularly noteworthy aspects of cirrus clouds: for example, in tropical regions, subvisual cirrus clouds occur sometimes in the tropopause. Cirrus cloud optical depths (cloud optical density, essentially the cross sectional area of the ice particles integrated from the top to bottom of the column) can be large, as would be the case for deep thunderstorm anvils, but they are observed most frequently with optical depths below 0.1 (Sassen et al. 2008; Kox et al. 2014).

A wispy layered cloud that forms at the top of a thunderstorm, termed an anvil because of its shape, is a cirrus that consists essentially of ice debris that spreads outward from the convective parts of the storm. Anvils do not include the white, dense portions of thunderstorms or the active convective column. Anvils can spread to form large, widespread cloud layers, especially in tropical areas, which can persist after their convective cloud source has disappeared.

The cirruslike low-level ice clouds and ice fogs of the Arctic are not considered cirrus. Nor are altocumulus clouds, which form in distinct layers, often less than 100 m thick, in the midtroposphere at about 5 to 8 km. They are identified from the ground as sharply outlined clouds reflecting their tendency to a liquid water composition containing rounded, often bubblelike convective elements. Cirrus often merge with altocumulus clouds, producing a deep ice-cloud layer.

Planetary-scale mapping of cirrus cloud occurrence and properties requires satellite remote sensing. However, it has proven to be difficult to detect cirrus clouds from space using passive radiance measurements, owing to their thin optical depth and their frequent occurrence as part of multilayered cloud systems (Sassen

et al. 2008). With the launch of the NASA *CloudSat* and *Cloud–Aerosol Lidar and Infrared Pathfinder Satellite Observation* (*CALIPSO*) in 2006, cloud observations from space entered a new era. Both satellites are part of the Afternoon Train (A-Train) constellation, with *CloudSat* carrying a cloud profiling radar and *CALIPSO* carrying a depolarization lidar [Cloud–Aerosol Lidar with Orthogonal Polarization (CALIOP); Stephens et al. 2002; Winker et al. 2009]. The near-simultaneous and coincident observations by a millimeter radar that can penetrate optically thicker clouds and a lidar that is sensitive to optically thin clouds have allowed vertically resolved profiling of cloud layers with an unprecedented accuracy (Mace et al. 2009). Since the launch of *CloudSat* and *CALIPSO*, many retrieval algorithms have been developed, and our knowledge on global cirrus distributions and characterization has greatly improved. In addition to active-only cloud observations from space, Delanoë and Hogan (2010) showed how additional assimilation of coincident infrared radiances from the Moderate Resolution Imaging Spectroradiometer (MODIS) can further improve the retrieval of ice cloud locations and their microphysical properties.

Cirrus clouds as observed from *CloudSat*/*CALIPSO* radar and lidar observations have been derived through a combined cloud boundary data product (Mace and Zhang 2014). In general, cirrus cloud tops are derived exclusively from CALIOP lidar backscatter data, owing to the characteristically small crystal sizes for which a millimeter radar is not sensitive. Cirrus cloud bases, in turn, are mostly detectable by both lidar and cloud physics radar (CPR) backscattering. Yet cloud radar data have proven their use for the detection of cirrus cloud bases, especially in relatively thick cirrus clouds that completely attenuate the lidar beam (optical depths larger than 3–5) (Sassen et al. 2008; Winker et al. 2010).

Sassen et al. (2008) define two basic criteria that must be satisfied to classify the detected cloud layers as cirrus, including a maximum visible optical depth τ of ≈ 3.0 and a maximum allowable cirrus cloud-top temperature of $-40°C$, the homogenous freezing point of pure water. Using this methodology, Sassen et al. (2008) found a global average frequency of cirrus cloud occurrence of 16.7% from the first year of *CloudSat*/*CALIPSO* data collected (Fig. 2-2), with a significant proportion of this cirrus cloud cover in the tropical and subtropical zonal belts (56% of the total cirrus coverage occurs within $\pm 30°$ latitude of the equator). Moreover, cirrus display a strong nocturnal frequency increase, in particular over land, of up to $\sim 30\%$ (Wylie et al. 1994; Sassen et al. 2009; see Fig. 2-3). Cirrus detections by *CloudSat*/*CALIPSO* further reveal the relatively high altitude of
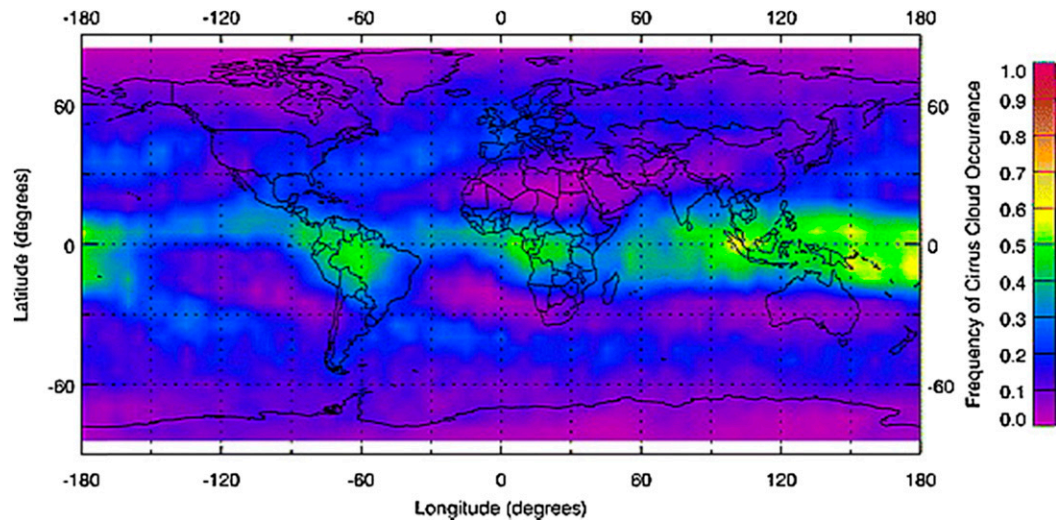
FIG. 2-2. Global distribution of average frequency of occurrence of cirrus clouds identified by *CloudSat/CALIPSO* within 5.0° lat × 5.0° lon grid boxes. These data are 1-yr averages of daylight and nighttime measurements and of single and multiple cirrus layers (from Sassen et al. 2008).

occurrence (Fig. 2-4), as expected from the results of other sources. Using *CALIPSO* data, Nazaryan et al. (2008) show that the maximum-occurrence frequency of up to 70% is found near the tropics over the 100°–180°E longitude band. They found a large latitudinal movement of cirrus cloud cover with the changing seasons. The examination of the vertical distribution of cirrus clouds shows the maximum of cirrus top-altitude occurrence frequency of approximately 11% at 16 km in the tropics.

A drawback of the polar-orbiting *CloudSat/CALIPSO* satellites is their limited temporal resolution, with a repeat cycle of 16 days. Observation of full cirrus life cycles is therefore limited. Kox et al. (2014) have shown how retrievals from *CloudSat/CALIPSO* can be complemented by measurements of the Spinning Enhanced Visible and Infrared Imager (SEVIRI) aboard the geostationary Meteosat Second Generation (MSG) satellite.

Their algorithm retrieves cirrus optical depths (between 0.1 and 2.5) and top altitude every 15 min, covers almost one-third of Earth's atmosphere, and is trained based on coincident *CALIPSO* retrievals.

As a result of their frequent occurrence, height in the atmosphere, and opacity (Sassen et al. 2008; Kox et al. 2014; see also Figs. 2-2–2-4), cirrus modulate the amount of solar radiative energy received by the climate system, reflecting a portion of the incident sunlight back to outer space. They also control the loss of energy to space by their effect on outgoing infrared radiation emanating from Earth's surface and lower atmosphere. Important feedbacks involving cirrus, their water content, and optical properties and their influences on climate have been proposed (Ramanathan and Collins 1991; IPCC 2013). Cirrus also play a vital role in Earth's energy budget through their effects on the surface albedo and generation of latent heat released in regions of ice
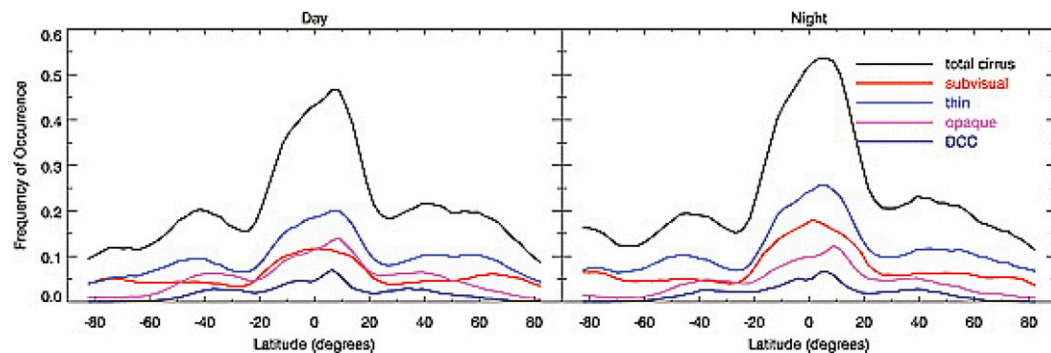

FIG. 2-3. Zonal average occurrence (%) for (left) day and (right) night of global total, subvisual, thin, and opaque cirrus clouds and of deep convective clouds (DCC) (from Sassen et al. 2009).
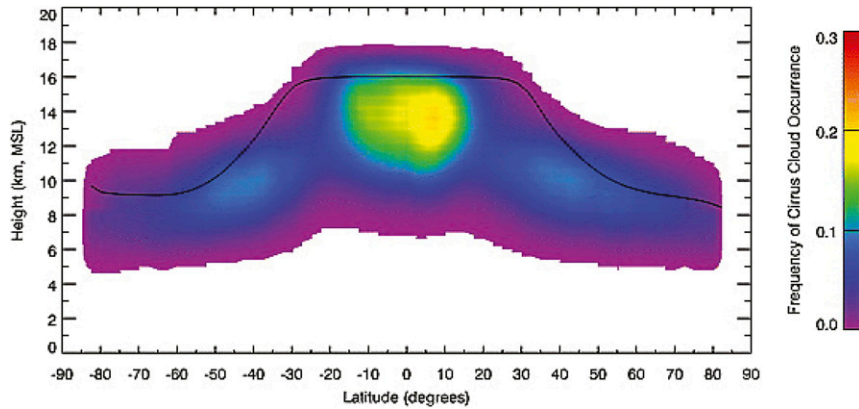
FIG. 2-4. Latitudinal distribution of identified heights of occurrence of cirrus clouds derived for 0.2-km height and 2.5° grid intervals. The line shows the mean tropopause heights averaged over the same 1-yr period, as taken from *CALIPSO* data files (from Sassen et al. 2008).

crystal growth. Cirrus clouds are also an important component of the planetary energy budget because of their large spatial extent and their strong interaction with radiation fields, both at solar wavelengths (visible light, below about 0.8 microns) and infrared (Ramaswamy and Detwiler 1986). The net radiation (infrared plus solar) is related to their optical depth. When cirrus clouds are thin enough that the sun can be seen through them, the net impact on the planetary radiation balance is generally warming; thicker cirrus reflect more sunlight and generally result in net cooling.

3. Cirrus formation mechanisms

Generally speaking, ice particles form after a moist parcel of air cools to the temperature at which the water vapor is supersaturated with respect to ice up to the onset point of ice nucleation. The supersaturation is produced primarily by lifting of the air parcel but can be maintained or enhanced by radiational cooling (Fusina and Spichtinger 2010). Lifting can occur on a large scale along a frontal boundary or by small-scale vertical circulations that develop in the vicinity of the core of the jet stream (Heymsfield et al. 1975; Heymsfield et al. 2010) or in convective clouds and gravity waves. In addition, cirrus clouds can form in layers that have dry or moist adiabatic thermal structures.

Cirrus cloud formation and development is in part influenced by radiative effects. Radiative cooling in moist upper-tropospheric layers can lead to cloud development in much the same way it leads to ground fog (Ramaswamy and Detwiler 1986). In addition, radiative heating, which usually warms the lower portions of a cirrus cloud, can warm the cloud layer and consequently produce convection (updrafts and downdrafts) and turbulence of sufficient strength to maintain or enhance the

layer. This is particularly relevant in tropical anvils. For example, Ackerman et al. (1988) found anvil average heating rates for 2-km-deep anvils is on the order of 20–30 K day^{-1}, leading to convective instability in the anvil, an effect studied by Lilly (1988) and others more recently. The radiative heating of thin tropical tropopause layer (TTL) cirrus, at altitudes from 14 to 18 km and also at low latitudes, has been estimated as sufficient to produce temperature increases of at least 2–3 K day^{-1} (Jensen et al. 1996; McFarquhar et al. 2000). As noted by Garrett (2008), observational studies suggest that TTL cirrus are often coincident with regions of deep convective cloud. Their numerical simulations demonstrated that an anvil cirrus spreads because strong absorption of thermal radiation and emission at cloud base and top creates horizontal heating gradients between the cloud and its environment. Durran et al. (2009) analytically and numerically examined the potential of this radiative heating on the TTL dynamics. They found that the layer exhibits rising motion, ~0.5 cm s^{-1}, and horizontal outflow from its top, producing gravity waves. These studies suggest that tropopause cirrus can affect climate indirectly by altering anvil cirrus dynamics.

The formation mechanisms of cirrus clouds differ according to the required supersaturations to form ice and the number of ice crystals that are produced. Classifying cirrus by means of the formation mechanisms leads to cirrus types characterized by physical parameters, besides those embedded in the terminology of the WMO (1956) for all cloud types (see section 2a), which are defined based on morphology derived from observations of visual appearance. Lynch et al. (2002) stated that particularly ice content, but also temperature, altitude, color ,and optical depth are relevant physical parameters for cirrus definitions, and some of these parameters can be deduced from the formation mechanisms (see also Sassen et al. 2002).
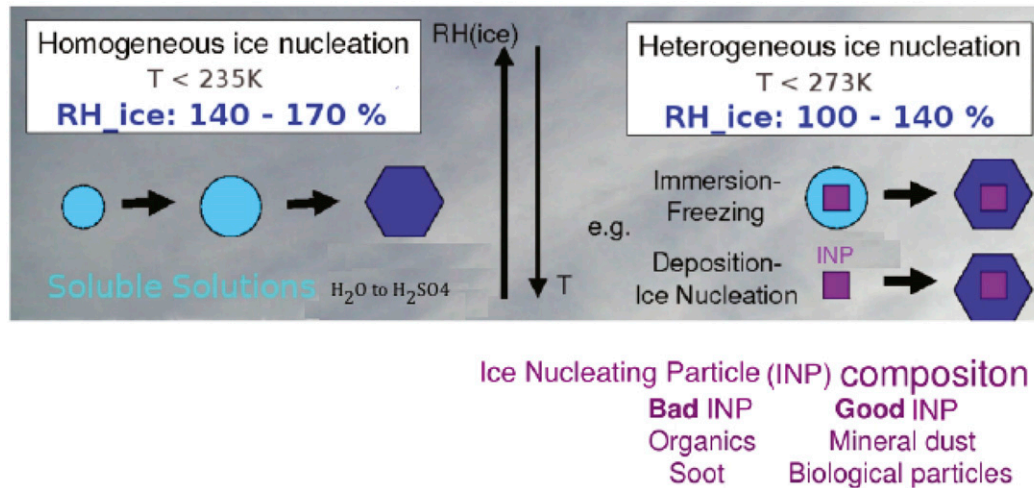
FIG. 2-5. Cirrus formation: two ways of ice formation determined by aerosol composition and supersaturation over ice.

Below a temperature of −38°C, activation of liquid water drops does not occur, since the relative humidity where ice forms is below water saturation (Heymsfield and Miloshevich 1993). At warmer temperatures, clouds can form via vapor deposition onto an ice nucleating particle (INP) or as liquid drops, which may freeze either heterogeneously due to an insoluble INP embedded in the droplet (see Kanji et al. 2017, chapter 1) or homogeneously without any insoluble inclusion at −38°C. These clouds can be partly or completely glaciated and are not cirrus clouds, but so-called mixed-phase clouds.

If a mixed-phase or all-liquid cloud is, however, lifted by atmospheric updrafts to altitudes with temperatures < −38°C, it is considered a cirrus. Luebke et al. (2016) and Krämer et al. (2016) classified this cirrus type as "liquid origin cirrus." They are found in the strong updrafts caused by deep convection [and are also called convective or anvil cirrus; Lynch et al. (2002); Sassen et al. (2002); Muhlbauer et al. (2014), Jackson et al. (2015)], but also in slower updrafts in connection to warm conveyor belts (Krämer et al. 2016).

At temperatures < −38°C, cirrus clouds are formed from insoluble or solution aerosol particles, either heterogeneously or homogeneously. This cloud type is classified as "in situ cirrus" by Heymsfield (1977). Krämer et al. (2016) summarized "in situ origin cirrus" as those cirrus types that are named in other studies "synoptic" in slow updrafts and "lee wave," "gravity wave," "orographic," or "jet stream" cirrus in faster updrafts (Lynch et al. 2002; Sassen et al. 2002; Muhlbauer et al. 2014; Jackson et al. 2015). In the next subsections, the heterogeneous and homogeneous in situ ice formation processes are described, while heterogeneous or homogeneous drop freezing—which leads to the liquid origin cirrus—is discussed in Cziczo et al. (2017, chapter 8).

a. Homogeneous and heterogeneous ice nucleation in cirrus clouds

Homogeneous freezing is the spontaneous formation of ice within a supercooled activated cloud droplet or a pure solution aerosol particle (see Fig. 2-5, left; note that the concentrated solution aerosol particles are also named haze droplets, since they have grown hygroscopically in high humidities). Droplets/drops freeze spontaneously at a temperature of −38°C, and freezing of solution droplets (haze particles) occurs at progressively lower relative humidities as the temperature decreases below −38°C (Heymsfield and Miloshevich 1993). The haze droplet that freezes homogeneously is also termed a homogeneous freezing nucleus (HFN). The process of homogeneous freezing is well defined and the subject of a comprehensive treatment by Koop et al. (2000), where it has been shown to be a function of the particle volume and water activity. It is important to note that at sufficient supersaturation all atmospheric particles may serve as HFN. However, atmospheric supersaturations are driven by the updraft of an air parcel and temperature. Hence, the number of ice crystals nucleated by homogeneous freezing increases with increasing updraft and decreasing temperature (Heymsfield and Miloshevich 1993). This is shown in Fig. 2-6, where concentrations of homogeneously nucleated ice crystals are calculated by Kärcher and Lohmann (2002) for a range of atmospheric updrafts. They found 0.001 to several hundreds of ice crystals per centimeter cubed with mean mass radii ranging between ∼100 and $3\,\mu$m, respectively (Krämer et al. 2016). However, observations show that the most frequent ice concentrations are around 0.1–1 cm^{-3} (Krämer et al. 2009). This could suggest that the updrafts where most
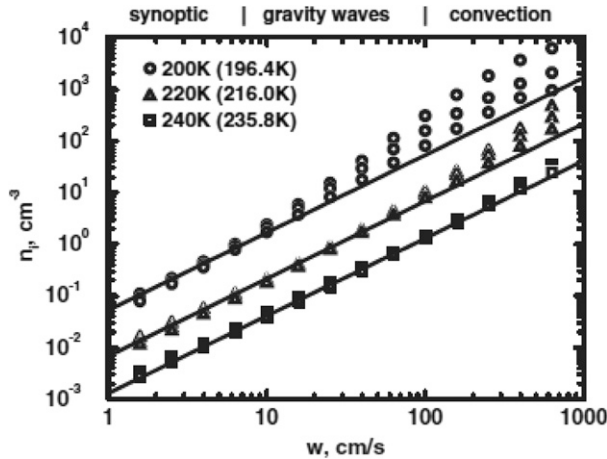
FIG. 2-6. Ice crystal number n_i dependence on vertical velocity w for purely homogeneous freezing (Kärcher and Lohmann 2002).

cirrus form are weak (see Fig. 2-6) or that heterogeneous ice nucleation often plays a role in the atmosphere.

Heterogeneous ice nucleation is more poorly understood than homogeneous freezing because there are several submechanisms by which ice is formed (see Fig. 2-5, right). Each of these submechanisms is fundamentally different from one another. Heterogeneous freezing can potentially begin as soon as the temperature is below 0°C and saturation of water vapor with respect to ice is reached. Heterogeneous ice nucleation requires a solid particle or inclusion, termed the INP [Pruppacher and Klett (1997); see also Kanji et al. (2017, chapter 1)]. The heterogeneous mechanisms that act in the cirrus temperature range are 1) immersion/condensation freezing and 2) deposition nucleation. 1) Immersion/condensation freezing is the formation of ice within an INP that is immersed in a shell of water that condensed while the air is cooling. There have been slight terminology differences based on the history of the immersed INP, but the two mechanisms are now considered synonymous. 2) Depositional freezing is the direct accumulation of ice on to the INP surface. A currently unresolved mechanism is "preconditioning" of an INP (Pruppacher and Klett 1997; Kärcher and Lohmann 2003; Wagner et al. 2016). In this case, a previous freezing cycle leaves some ice on or within a particle that then leads to more rapid ice formation if a suitable temperature and saturation are again reached. Heterogeneous freezing is affected by the size, surface composition, and morphology of the INP (Pruppacher and Klett 1997). DeMott et al. (2003) and DeMott et al. (2010) have shown INPs are rare in the background free troposphere, 10–100 L^{-1} (0.01–0.1 cm^{-3}), but with extremely limited measurements below −38°C; at warmer temperatures the INP concentration can be related to the

presence of aerosol larger than 0.5 μm (DeMott et al. 2010). Some INPs can be referred to as relatively "good" and others as relatively "bad"; examples of each are listed in Fig. 2-5 (right panel), with a quantitative representation given in Cziczo et al. (2013).

A cirrus cloud that forms heterogeneously is therefore expected to be different from one that forms homogeneously, especially in updrafts $\geq 10\,cm\,s^{-1}$, because it would contain <100 ice crystals (i.e., no more than the concentration of INPs in the initiating cloud parcel). Even with weaker updrafts, the ice crystal concentrations and sizes are modulated in the presence of INPs (Kärcher and Lohmann 2003; Spichtinger and Cziczo 2010). The effect of INPs on ice crystal concentrations is in most cases fewer ice crystals than due to pure homogeneous freezing. However, in very low updrafts, where homogeneous freezing produces only few ice crystals, heterogeneous freezing can create more ice crystals when the INP number exceeds the homogeneously formed ice (Kärcher and Lohmann 2003). Consequently, the sizes of the ice crystals are smaller when more ice crystals are produced, while fewer nucleated ice particles results in larger crystals.

Thus, the characterization of INPs, in particular in the cirrus temperature range, is one of the important open questions in the field of ice cloud research. This knowledge gap can be traced back to instrumentation capable of operating at ambient temperatures and/or sampling the complete size distribution of ice crystals.

b. Atmospheric importance of cirrus freezing mechanisms

The important aspect of atmospheric ice nucleation is that heterogeneous ice nucleation mechanisms are active at lower supersaturations (i.e., before homogeneous freezing) (Fig. 2-5). That is to say a parcel reaching homogeneous freezing must first pass through temperatures and saturations sufficient to cause heterogeneously formed ice. This has been considered by researchers such as Kärcher and Lohmann (2003), Kay et al. (2006), and Krämer et al. (2016). The combination of INP abundance, its freezing supersaturation, and how rapidly a trajectory is traversed (i.e., the vertical velocity) determines where and by what mechanism a cirrus cloud forms and thus also which microphysical properties, such as ice crystal number and size, ice water content, and shape and surface texture of ice crystals, the cloud has.

This is important since these microphysical properties of cirrus, for example, regulate the vertical redistribution of water from sedimenting ice crystals in the upper troposphere and, consequently, the water exchange with the lower stratosphere (Krämer et al. 2016). The upper-troposphere/lower-stratosphere region is especially
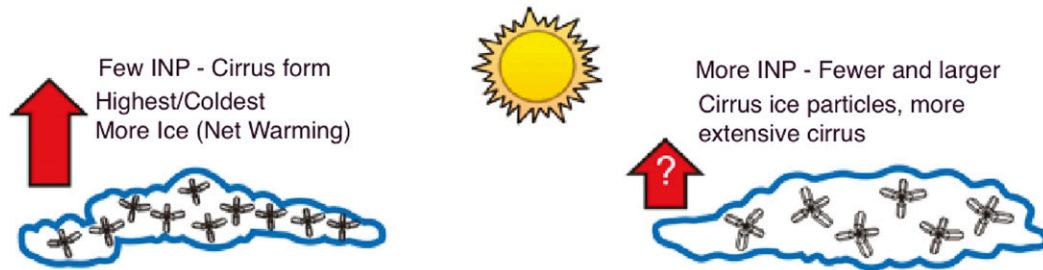
FIG. 2-7. The effect of the number of ice nuclei on cirrus cloud coverage and radiative effects (from DeMott et al. 2010).

sensitive to even small changes in water vapor, since it is a greenhouse gas, and radiative transfer calculations show that the small mass of water vapor in the lower stratosphere plays a significant role in controlling surface temperatures (see, e.g., Riese et al. 2012).

Further, to define the impact of cirrus on Earth's radiative budget (see section 5), it is critical to determine how the microphysical and thus radiative properties of ice particles in cirrus depend on environmental conditions and formation mechanisms. DeMott et al. (2010) provided a sketch on the possible relation between INP number, cirrus appearance, and radiative feedback of the cirrus clouds (Fig. 2-7): in case only few INPs are available (left panel), the few formed ice crystals cannot efficiently deplete the water vapor, and the supersaturation increases until homogeneous ice nucleation occurs and a cirrus with many small ice crystals forms at high and cold conditions. These thin cirrus have a net warming effect. If more INPs are available (right panel), heterogeneous freezing produces a lower, warmer, and thicker cirrus with fewer but larger crystals, which efficiently reduces the supersaturation so that homogeneous ice nucleation is suppressed (Krämer et al. 2016). The net radiative effect of such cirrus is unknown. Thus, it is obvious that dependencies are needed to develop and evaluate parameterizations of ice cloud properties for models with a myriad of different spatial and temporal scales and for evaluation of the model results themselves. Observations of ice cloud properties can be obtained from both in situ observations and remote sensing retrievals, the latter of which require in situ observations to evaluate assumptions used in the retrieval schemes.

The ice water content and distributions of ice crystal sizes and shapes are the most important microphysical quantities for determining how cirrus impact radiative heating (e.g., Ackerman et al. 1988; Macke et al. 1996) and for developing an understanding of the microphysical and dynamical processes occurring in cirrus. In addition, distributions of crystal aspect ratios (Fu 2007; Um and McFarquhar 2007; Yang and Fu 2009) and

knowledge of single-scattering properties (e.g., Takano and Liou 1989; Yang et al. 2005) and ice crystal surface roughness (Yang et al. 2003) are needed for quantifying the radiative impact. Although many prior studies have measured distributions of ice water content (IWC) (Schiller et al. 2008; Luebke et al. 2013; Heymsfield et al. 2013; Krämer et al. 2016), ice crystal sizes (Heymsfield and Platt 1984; McFarquhar and Heymsfield 1996, 1997, 1998; Ivanova et al. 2001; Boudala et al. 2002; Field and Heymsfield 2003; McFarquhar et al. 2007a; Field et al. 2007), of crystal habits (Heymsfield and Miloshevich 1995; Korolev et al. 1999; Gallagher et al. 2005; Um and McFarquhar 2009), and of aspect ratios (Auer and Veal 1970; Hobbs et al. 1974; Davis 1974; Mitchell and Arnott 1994; Baker and Lawson 2006; Um et al. 2015) in different environmental conditions, there are few comprehensive studies that have identified the manner in which the nucleation mechanism or cirrus formation mechanism controls these ice crystal properties. A larger database where properties are examined as a function of meteorological or crystal formation mechanisms (e.g., Muhlbauer et al. 2014; Jackson et al. 2015; Krämer et al. 2016) is still needed to understand how different growth processes and formation mechanisms control the microphysical and radiative properties.

4. Microphysical properties

The most important microphysical quantities of cirrus clouds are (besides crystal aspect ratios, single-scattering properties, and surface roughness) the IWC, the ice particle size distributions (PSD), and their shapes. Characteristics of cirrus IWC, ice particle size distributions, and associated size spectral moments (median diameter and ice water content) have been reported in a number of studies. Korolev et al. (2001) present a large set of observations in continental stratiform cirrus clouds over eastern Europe at temperatures from $-30°$ to $-50°C$. The IWC was measured with a Nevzorov total water content probe and the volume extinction coefficient with an extinctiometer. Median

values of the IWC decreased from $0.011\,\mathrm{g\,m^{-3}}$ in the temperature range $-40° < T < -30°\mathrm{C}$ to $0.007\,\mathrm{g\,m^{-3}}$ for $-50° < T < -40°\mathrm{C}$. Cumulative probability distributions of the IWCs in these temperature intervals for these temperatures are presented in Fig. 5a of Korolev et al. (2001). Note that these IWCs may be somewhat underestimated because the IWC measurements were made with the older Nevzorov cone, not the updated deep dish cone that reduces the amount of ice that bounces out of the cone (Korolev et al. 2013). Also note that the probe measures IWCs in the range of about 3×10^{-3} to $2\,\mathrm{g\,m^{-3}}$; thus, IWCs below the instruments' detection threshold suggest that the median values may be overestimated (see discussion below). The most globally diverse datasets are from the studies of Heymsfield and McFarquhar (2002), Schiller et al. (2008), Luebke et al. (2013), Heymsfield et al. (2013), and Krämer et al. (2016). These include data from the Arctic, midlatitude Northern Hemisphere, and tropical Northern and Southern Hemisphere regions. Altitudes extend to almost 19 km and sampling temperatures to $-86°\mathrm{C}$. An overview of these cirrus properties will now be given, followed by a section describing the feedback of cirrus clouds on climate.

a. Ice water content

Two studies that collected a large number of direct measurements of the IWC in diverse geographical areas are summarized here. Krämer et al. (2016) compiled a set of direct measurements of the IWC from 17 field programs over Europe, Africa, the Seychelles, Brazil, Australia, the United States, and Costa Rica, totaling 94 h of in situ data. The geographical range is from 75°N to 25°S, and the temperature range is from $-25°$ to $-91°\mathrm{C}$. Heymsfield et al. (2016) reported the direct measurements of the IWC derived from 10 aircraft field programs over North and Central America, the Caribbean, and Australia, spanning latitudes from the Arctic to the tropics and temperatures from $-86°$ to $0°\mathrm{C}$. This dataset contains about 260 000 data points, averaged over 5-s intervals, with an in-cloud pathlength of about 260 000 km. To examine both the temperature dependence of the IWC and its variability, we have used their original data to derive probability distribution functions (PDFs) of the IWC as a function of temperature. Within the 10°C temperature increments shown in Fig. 2-8, the IWC displays considerable variability, the result of different formation mechanisms (Krämer et al. 2016), geographical location (Heymsfield et al. 2016), and presumably life cycle. The median values of the IWC in each temperature interval, listed at the top of each panel in Fig. 2-8, indicate that the IWC increases with temperature. The rather large differences between the Krämer et al. (2016) and Heymsfield et al. (2016) studies has to do in part with the

former study focusing more on stratiform clouds and the latter more on convective clouds. Some of the difference is also due to differences in the IWC measurement ranges of the instruments used in those studies.

The in situ observations have an inherent sampling bias in that they are usually directed toward measuring specific types of clouds and, more generally, clouds that are in their active, rather than decaying, stages. For that reason and to gain a more comprehensive structure, we draw upon ice water contents globally retrieved by *CloudSat* over a 6-yr period. The *CloudSat* Ice Cloud Property Product (2C-ICE) contains retrieved estimates of the IWC for identified ice clouds measured by the *CloudSat* CPR and the *CALIPSO* lidar. This 2C-ICE cloud product uses combined inputs of the measured radar reflectivity factor from *CloudSat* and measured attenuated backscattering coefficients at 532 nm from the *CALIPSO* lidar to constrain the ice cloud retrieval more tightly than the radar-only product. Temperature is derived from the ECMWF auxiliary (ECMWF-AUX) temperature product. According to the authors, this generates more accurate results, particularly at the lower temperatures (Deng et al. 2015). We will address that point below. Note that, as with any retrieval algorithm, there are inherent uncertainties; the retrieval accuracy is examined using case studies (Deng et al. 2013) and statistics (Heymsfield et al. 2016).

Using the 2C-ICE stratiform and convective cloud flags, Fig. 2-9 shows the probability distribution function of IWC as a function of temperature, partitioned by stratiform and convective clouds (Figs. 2-9a and 2-9b, respectively). Because the dataset is extremely large, it is possible to derive PDFs in 1°C temperature increments, thereby eliminating variance in the PDFs due to the $\pm5°\mathrm{C}$ temperature increments necessary for the in situ data. In Table 2-1, the median IWCs for all ice cloud situations and the separation according to stratiform and convective situations are listed.

The retrieved IWCs show a strong increase with temperature and wide variability at a given temperature, even for each cloud formation type (Figs. 2-9a,b). On average, the IWCs, particularly at the higher temperatures, are larger than for the in situ observations, although the spread is just as wide. Of particular note is that at the lowest temperatures, $\sim -85°\mathrm{C}$, the IWCs from the in situ observations (Fig. 2-9) are peaked at about an order of magnitude lower than the 2C-ICE distribution. This comparison suggests that the 2C-ICE product is missing a significant portion of the very thin, subvisual cirrus that was observed from the in situ observations.

Figure 2-10 uses the 2C-ICE product to derive the latitudinal dependence of the IWC for constant temperatures of $-70°$ to $-30°\mathrm{C}$ in 10°C temperature
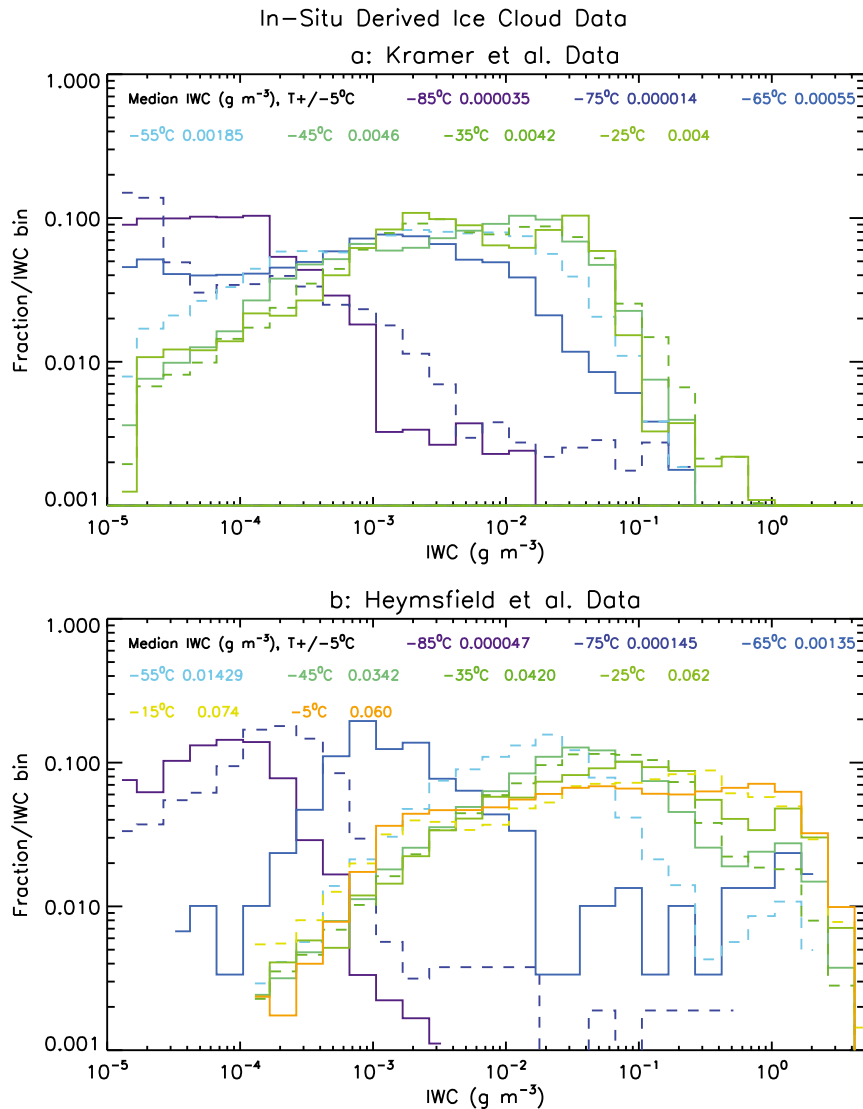
FIG. 2-8. Probability distributions of the ice water content measured in 10°C increments of temperature, with median values per 10°C listed in the top of each panel: (a) from the original data reported in Krämer et al. (2016) and (b) from the original data reported in Heymsfield et al. (2016).

increments. For stratiform and convective clouds combined, there is a dependence of the median IWC on latitude, with the highest values in the equatorial regions and the lowest in the polar regions (Fig. 2-10a). When convective clouds only are considered, a much stronger dependence on latitude is noted, with relatively high IWCs found in the tropical regions (Fig. 2-11a).

b. Cirrus ice crystal concentrations and size distributions

Many prior studies have measured size distributions in ice clouds. However, most of the earlier studies that reported cirrus crystal concentrations did not consider the artificial amplification of small crystal concentrations due to large crystal shattering on probe tips and are thus unreliable and should be used with caution [see Baumgardner et al. (2017, chapter 9) and articles by Korolev et al. (2011, 2013) and Jackson et al. (2014)]. Data acquired with the use of redesigned probe tips (Korolev et al. 2011) and those that use processing algorithms to eliminate artifacts (Field et al. 2006) are more reliable. Although Jackson and McFarquhar (2014) showed that higher-order moments derived from measurements in ice clouds are not significantly biased by shattering, quantities based on lower-order moments, such as total concentration and size distributions for

CloudSat Retrievals, Ice Cloud Data

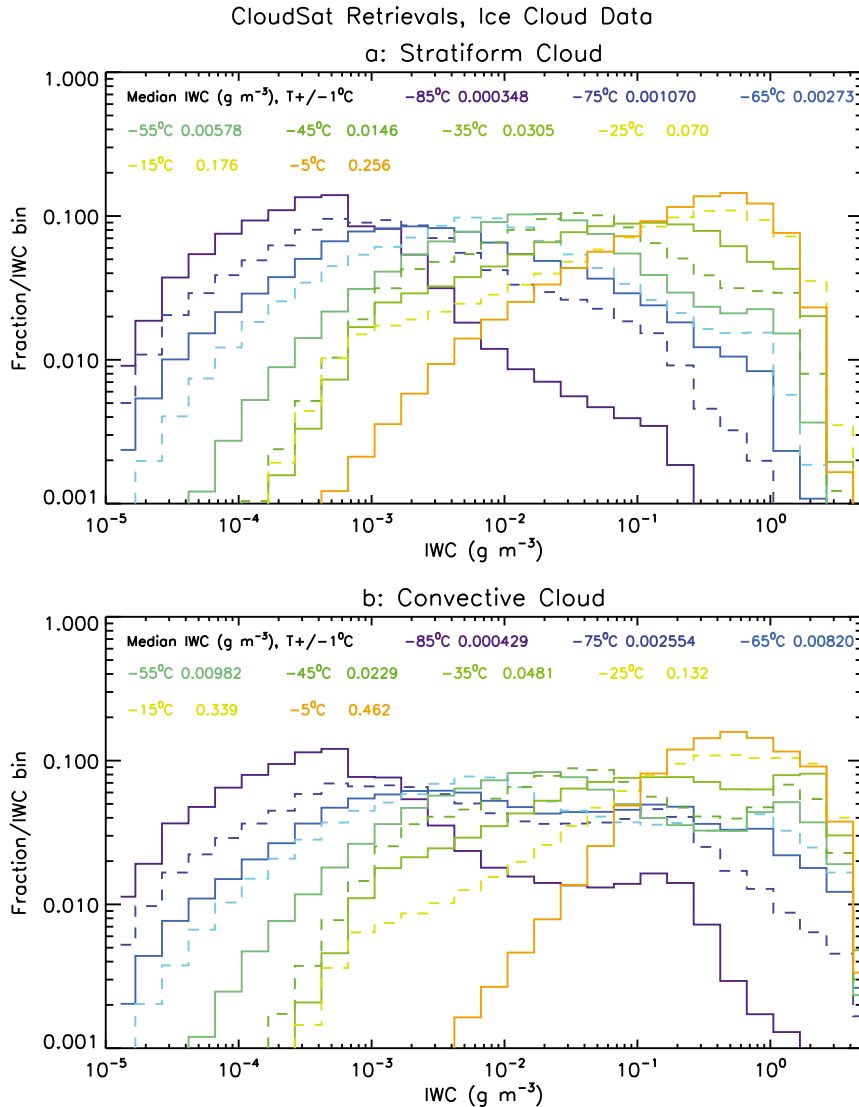### a: Stratiform Cloud

b: Convective Cloud

FIG. 2-9. Probability distributions of the ice water content retrieved from the *CloudSat* 2C-ICE product for the period 2006–10. Each PDF is for a 1°C temperature interval over the temperature range shown. (a) For ice clouds flagged as stratiform. (b) For convective clouds.

diameter $D < 200\,\mu\text{m}$, that did not use corrections for shattering or redesigned probe tips are suspect. A complete discussion of measurement issues and uncertainties is given in McFarquhar et al. (2017, chapter 11).

Ice crystal sizes generally increase downward in a cirrus cloud layer (Fig. 2-11) and as the temperature increases (Fig. 2-12). The PSD appear to fit well to gamma functions or exponential functions (e.g., Gunn and Marshall 1958; Wong et al. 1988; Heymsfield et al. 2002; McFarquhar and Black 2004; McFarquhar et al. 2007a; Heymsfield et al. 2009, 2013; Mitchell et al. 2010; Muhlbauer et al. 2014). The cirrus total ice concentrations generally fall in the range $5–500\,\text{L}^{-1}$, with a gradual decrease noted with increasing temperature. Exceptions are noted in convective

regions (temperatures below −40°C) and cirrus anvils and other situations that result from strong updrafts, where much larger concentrations have been observed (see Heymsfield et al. 2009). On average, the size distributions broaden with temperature, with larger and more numerous particles observed in the clouds that are associated with convection or that originate from liquid water regions (liquid origin), that glaciated as determined from liquid water sensing probes on the research aircraft (Fig. 2-12a) or from analysis of backward trajectories (Fig. 2-12b). In stratiform cirrus regions, where the cirrus-forming updrafts are relatively weak, the largest particles can still attain 1 mm or larger. These cirrus clouds can be the remnants of convection that has long since dissipated,

TABLE 2-1. Median values of the ice water content (g m^{-3}) in given temperature intervals from the in situ data and from *CloudSat* retrievals.

In situ data									
T (°C)	−90 to −80	−80 to −70	−70 to −60	−60 to −50	−50 to −40	−40 to −30	−30 to −20	−20 to −10	−15 to −5
Krämer et al. (2016)	0.000 035	0.000 014	0.000 56	0.001 85	0.0046	0.0042	0.0037	—	
Heymsfield et al. (2013)	0.000 047	0.000 150	0.0014	0.014	0.034	0.042	0.062	0.074	0.059
CloudSat									
T (°C)	−86 to −84	−76 to −74	−66 to −64	−56 to −54	−46 to −44	−36 to −34	−26 to −24	−16 to −14	−6 to −4
All	0.000 17	0.000 30	0.0007	0.001 83	0.0045	0.009	0.015	0.019	0.034
Stratiform	0.000 35	0.0011	0.0027	0.0058	0.015	0.031	0.067	0.176	0.26
Convective	0.000 43	0.0026	0.0082	0.0098	0.023	0.048	0.13	0.34	0.46

but displaying a tendency for larger particles [the region from the Stratospheric–Climate Links with Emphasis on the Upper Troposphere and Lower Stratosphere (SCOUT) in Fig. 2-12a, lower panel]. The largest particle size in the measured PSD increases from about 50 µm to above 1 mm over the −86° to −40°C temperature range.

McFarquhar et al. (2015) showed that parameters of derived gamma distributions can depend on the algorithm used to fit the data. They explained the parameters' dependence on fit algorithms through the sensitivity to parameters on the tolerance permitted by the fit algorithms, meaning a volume of equally realizable solutions in the phase space of gamma fit parameters is needed to characterize PSDs. They derived a technique to construct these volumes, taking into account both the codependence of the fit parameters and the statistical uncertainty of the measured PSDs. Jackson et al. (2015) used this technique to examine how PSDs measured over Oklahoma during the Small Particles in Cirrus (SPARTICUS) experiment varied with temperature and cloud formation mechanism, also showing that multimodal distributions were sometimes needed to characterize PSDs (Fig. 2-13). Consistent with prior studies of Mitchell et al. (1996) and Lawson et al. (2010), they hypothesized that the smaller mode corresponded to particles growing by vapor diffusion or homogeneous nucleation, whereas particles in the larger mode grow by diffusion and aggregation. Differences between the SPARTICUS PSD and those measured by Heymsfield et al. (2013) could be associated with the different geographic locations or the weaker updrafts in the tropical cirrus measured by Heymsfield et al. (2013). This shows that further studies are needed to stratify measured PSD by temperature, location, formation mechanism, updraft strength, aerosol concentration, and other environmental conditions to better understand the controls of cirrus properties and to examine whether normalized PSD are less sensitive to such changes (e.g., Delanoë et al. 2005).

c. Cirrus cloud evolution

Few studies have characterized the evolution of cirrus clouds. Heymsfield (1975a,b,c) studied the evolution of the ice particle size distributions in cirrus uncinus and cirrostratus clouds using a combination of aircraft measurements at different altitudes and Doppler radar observations, together with a 1D parcel model. In cirrus uncinus source regions (the generating cell head), crystals were found to be nucleated in the upwind portion of the head (the updraft) before being carried into the trail region of the head downshear (the downdraft) as a result of wind shear. Ice particles grew in the ice supersaturated regions below the head and then sublimated in the relatively dry regions below. Ice nucleation was observed to occur near the cloud top; crystals sedimented and grew from this source region near the top to near the base and sublimated to the base. Garrett et al. (2005), and more recently Frey et al. (2011), examined the evolution of a cirrus anvil. Ice crystals smaller than 50 µm dominated the size distributions and radiative properties. In the anvil, ice crystals larger than 50 µm aggregated and precipitated, thereby resulting in an increasing dominance of small ice crystals. Aggregation and fallout led to a decrease in the ice water contents and ice crystal effective radii with time.

Lagrangian spiral descents, where an aircraft descends at about 1 m s^{-1}, about the same velocity as the larger particles in the size distributions, have been used to characterize the change in the slope and number concentration of the ice particle size distribution (Heymsfield et al. 2002; McFarquhar et al. 2007b). In the growth regions of the clouds, the slopes of the PSD increase and the number concentrations decrease, largely because of aggregation. The smaller particles are swept out by the larger ones, leaving relatively smaller particles up higher in the cloud layer and larger but fewer particles in the lower regions.
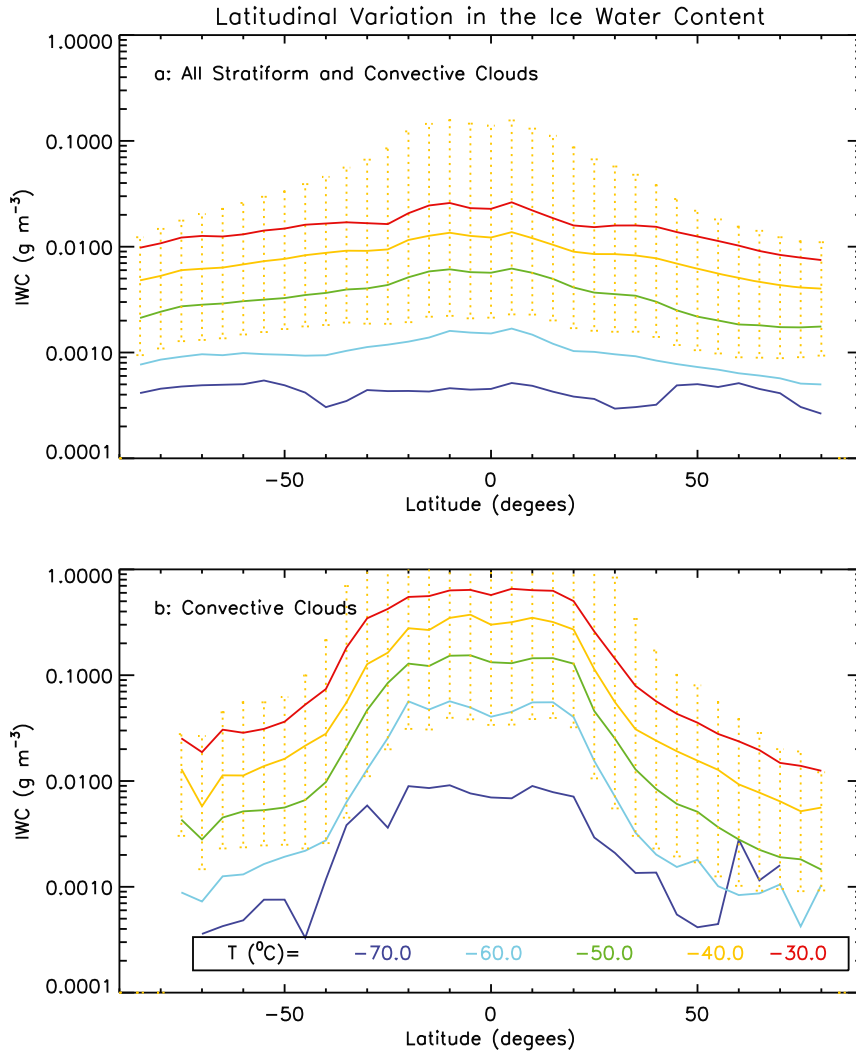
FIG. 2-10. Ice water content as a function of latitude, partitioned by temperature as derived from the *CloudSat* 2C-ICE retrieval product. Colored lines represent different temperatures, and dotted lines are the ± 1 standard deviation for a temperature of $-40°C$. (top) Stratiform and convective clouds. (bottom) Convective clouds.

Even with these observations, it is problematic to measure the evolution of cirrus cloud microphysics from in situ observations for several reasons. First, the in situ aircraft may alter the clouds that are being sampled. Second, except for anvil cirrus, it is very difficult to identify when a cirrus cloud is first forming. With satellite active remote sensors (*CloudSat* and *CALIPSO*), it is impossible to measure the evolution because the sensors on these satellites only take a snapshot of a single cloud. The options for measuring cirrus cloud evolution include ground-based or aircraft-borne active remote sensors that try and track cirrus from its inception through decaying stages, but this is operationally difficult to do, and the microphysical retrieval algorithms have inherent uncertainties.

The primary way in which evolution can be studied is with a cloud or mesoscale model, although this has inherent uncertainties. Starr and Cox (1985) used a cloud model to investigate the role of various physical processes on the life cycle of cirrus clouds. They found that, although the magnitude of large-scale ascent is critically important in determining the bulk physical properties of cirrus, the effects of the resulting microphysical composition (size distributions and crystal habits) affect the larger ice crystals and thus the mean descent velocity of the ice crystal populations. Radiative properties affect the local buoyancy and hence the structure and bulk properties of the cirrus and produce significant differences in the cirrus properties between midday and night times. Khvorostyanov and Sassen (1998), using a 2D
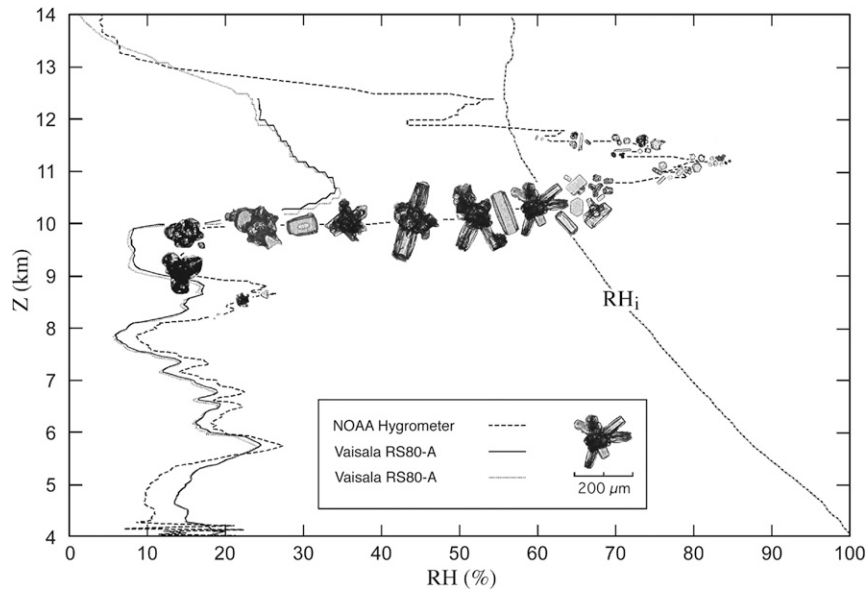
FIG. 2-11. Pictorial depiction of the growth of cirrus crystals downward in a cirrus cloud layer, using ice crystal replicator data collected from a balloon-borne system in a cirrus cloud with a top temperature of −43°C (from Miloshevich and Heymsfield 1997). The largest crystals are about 300 μm in diameter. The lines show the relative humidity with respect to water saturation as measured with three different instruments, and a fourth line (labeled RH$_i$) shows the relative humidity with respect to saturation with respect to ice and the temperature at each level.

model with explicit microphysics and radiation, modeled developing cirrus clouds generated in a stable atmosphere by relatively slow, synoptic-scale ascent. They found that the process of vapor deposition to ice crystals and the eventual depletion of the supersaturation in cirrus is far from instantaneous, varying from 0.5 to 3 h. They found that cooling in the upper part of the cirrus and heating in the lower part are appreciable. They also found that the decrease in the shortwave radiative balance (albedo effect) for their simulated cirrus cloud exceeded the net gain in longwave balance (greenhouse effect) near local noon, attributing it to the abundance of small crystals in the upper cloud regions.

The dependence of cirrus evolution on the initial formation mechanism in terms of microphysical and radiative properties has been studied by Joos et al. (2014) and Kuebbeler et al. (2014). Joos et al. (2014) used the large-eddy simulation Eulerian or Lagrangian model (EULAG) to perform idealized simulations with different concentrations of INPs in a dynamically dominated regime with high vertical velocities. They showed that, even under these conditions, low number concentrations of INP on the order of 0–50 L^{-1} are able to strongly decrease the simulated ice crystal number burden, the ice water path, and optical depth of the cloud. The shortwave, longwave, and net cloud forcings are also reduced with increasing INP concentrations.

Kuebbeler et al. (2014) studied dust ice nuclei effects on cirrus clouds by applying a multiple-mode ice microphysical scheme to the general circulation model ECHAM5. Similar to Joos et al. (2014), they found that heterogeneous nucleation on efficient mineral dust particles and the consideration of preexisting ice in the nucleation process may lead to a global reduction of ice crystal number and mass by 10% and 5%, whereas the ice crystals' size is increased by 3%.

d. Cirrus ice crystal shapes

Weickmann (1948) reported the earliest airborne investigations of the microstructure of cirrus clouds. From ice crystals collected using an open-cockpit aircraft, he found that the primary crystalline forms in cirrus with the stronger vertical motions (e.g., cirrus uncinus) were either hollow hexagonal columnar shapes or three-dimensional clusters of prismatic crystals joined at a common center (bullet rosettes); with weaker vertical velocities (e.g., cirrostratus) they were primarily hexagonal columns and plates. More recent observations indicate that ice particle habits are dependent upon the temperature and ambient relative humidity. Laboratory experiments of Bailey and Hallett (2004) indicate that, from −20° to −40°C and at ice supersaturations in excess of 2%, the most frequent habits observed were platelike polycrystals and plates, the complexity

a: Based on Heymsfield et al. (2013) study

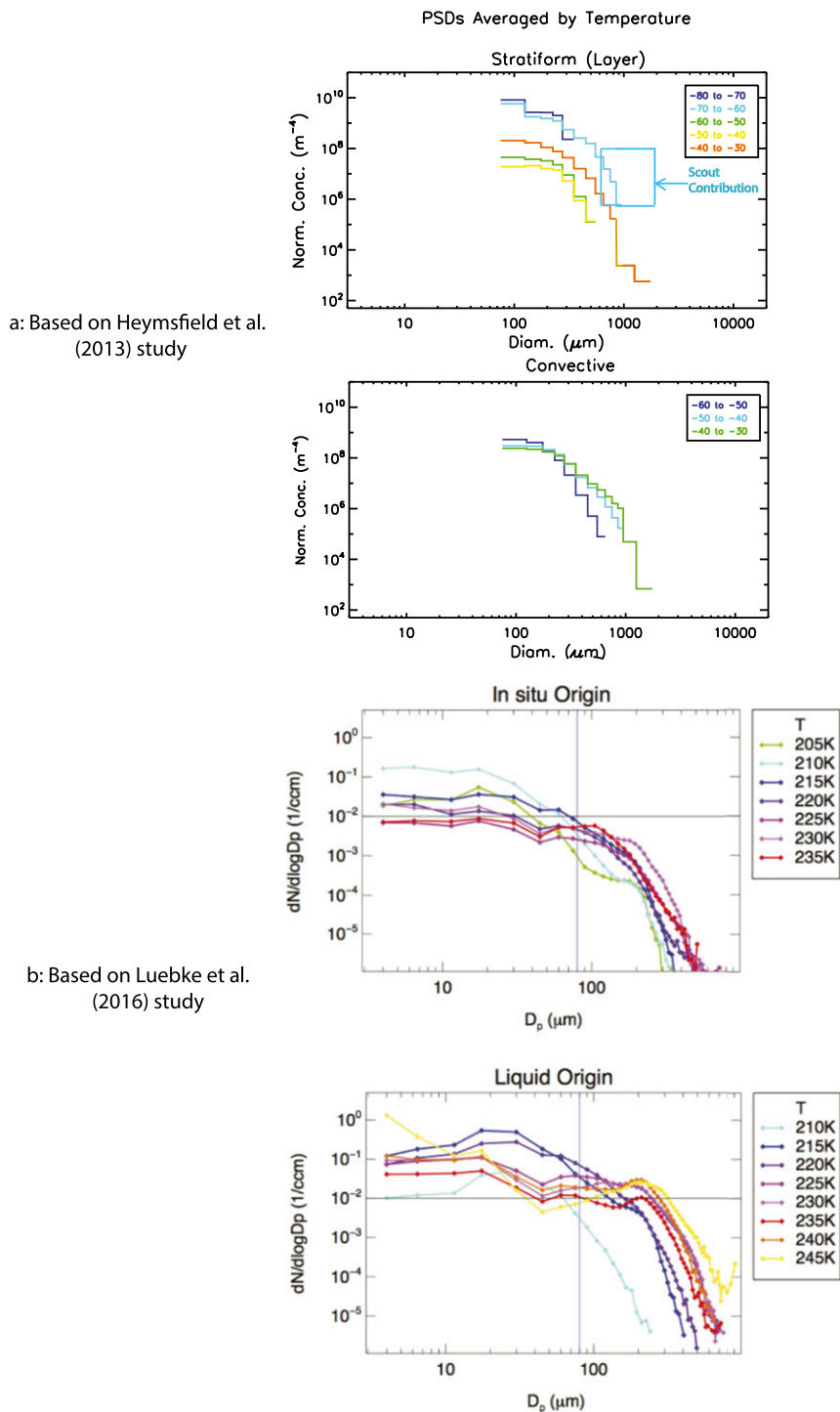b: Based on Luebke et al. (2016) study

FIG. 2-12. Cirrus ice PSD, in the form of concentrations measured per size bin normalized by the bin width, averaged in the specified temperature intervals corresponding to cirrus cloud forming temperatures. The PSD are based on (a) the dataset presented in Heymsfield et al. (2013) and (b) from Luebke et al. (2016). (top) PSD in (a) and (b) are from cirrus clouds formed in situ by layer lifting; (bottom) PSD in (a) are from cirrus clouds generated by deep convection but detrained and with no liquid water and in (b) are thick cirrus clouds originating from mixed-phase clouds but with no liquid water (liquid origin).
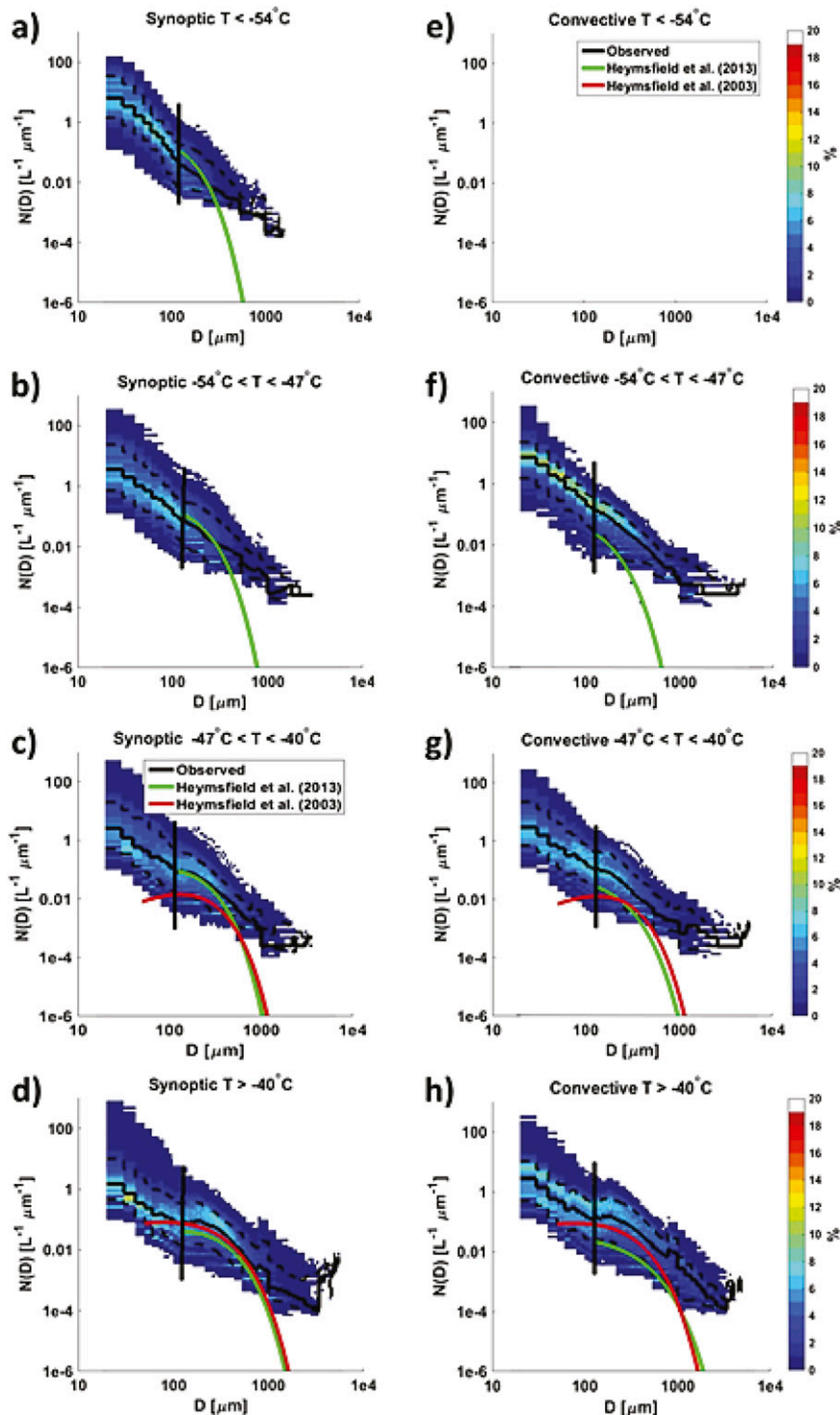
FIG. 2-13. Normalized distribution of $N(D)$ (%) for all (left) synoptic and (right) convective cirrus during the SPARTICUS field program when (a)(e) $T < -54°C$, (b)(f) $-54° < T < -47°C$, (c)(g) $-47° < T < -40°C$, and (d)(h) $T > -40°C$, from Jackson et al. (2015). The solid black horizontal line denotes the median; dashed lines denote 10th and 90th percentiles of $N(D)$. Solid colored lines show Heymsfield et al. (2013) curves. The solid vertical black line shows the mean location of the boundary between the first and second modes. Colors represent normalized frequency.

of forms increasing with increasing supersaturation. Colder than −40°C, a marked shift to columnar behavior was found, except at low to moderate ice supersaturation (<10%), where the habit is essentially the same as at warmer temperatures with a small increase in the frequency of short columns. At moderate ice supersaturation (10%–25%), long solid columns and polycrystals with columnar and platelike components were found. Above approximately 25% ice supersaturation, bullet rosettes, long columns, and column-containing polycrystals are observed, the frequency of bullet rosettes and columns increasing with increasing ice supersaturation. At −60°C and colder, needle forms appear along with columnar forms. In situ observations indicate that cirrus particles, especially bullet rosettes, can collect together to produce aggregates of crystals, leading to most of the crystals observed at sizes above $500\,\mu$m.

The laboratory findings are the result of ice crystal growth at constant temperatures and relative humidities, but in nature cirrus crystals encounter varying temperatures and relative humidities during growth and sublimation. Korolev et al. (1999) suggested that such cyclic growth may lead to the formation of irregular ice, and the same authors concluded that the majority of ice particles in midlatitude stratiform clouds observed during several campaigns had irregular shapes. Nelson and Knight (1998) suggested that irregular shapes may arise as a result of the asymmetry between the dynamic processes involved in growth and sublimation. Recent laboratory experiments where ice crystals were subjected to several growth cycles indeed led to progressively increasing complexity (Chou et al. 2014).

Both in situ and remote sensing measurements carried out over the last few years indicate that cirrus ice crystals typically depart from the simple, idealized geometry based on smooth hexagonal shapes, indicating complexity and/or surface roughness. The most obvious manifestation of this departure is in the relative rarity of the 22° halo, which tends to be infrequent at most geographical locations, with the exception of the Antarctic and Arctic, where diamond dust is relatively common, for example (Yang and Liou 1998; Mishchenko and Macke 1999; Ulanowski 2005). Despite the apparently minor difference in terms of ice crystal appearance, surface roughness can have a dramatic influence on the scattering properties and, hence, the radiative properties of cirrus. The halo visibility, as quantified by the so-called halo ratio, and the scattering asymmetry parameter g measured in situ were found to be positively correlated (Auriol et al. 2001; Gayet et al. 2011). Haloes were also more likely for smaller crystal sizes and for those with more compact shapes (Um and McFarquhar

2015). Smooth ice analogs had higher asymmetry parameters than their rough counterparts (Ulanowski et al. 2006), and the same was the case for modeled scattering (Yang et al. 2015). This means that, at wavelengths that can interact with the given roughness scale, rough ice crystals can be significantly more reflective than smooth ones, potentially shifting radiative forcing by cirrus toward lesser warming.

While the fine detail of ice crystal geometry is currently beyond the reach of imaging cloud probes (Ulanowski et al. 2004; Connolly et al. 2007; Bailey and Hallett 2004), indirect information can be obtained by means of various light-scattering probes or using remote sensing. Typically, aircraft and satellite measurements of cirrus radiances show featureless phase functions, which are not consistent with the idealized geometries (Foot 1988; Baran et al. 2001; Baran 2004; Garrett 2008; Baran 2012). Gayet et al. (2011) found prevalent particles with imperfect or complex shapes at the trailing edge of midlatitude frontal cirrus. For one full day of Polarization and Anisotropy of Reflectances for Atmospheric Sciences (PARASOL) data over ocean, very rough faceted particles provided an improved fit to polarized reflectances (Cole et al. 2013). In a study by Baum et al. (2011), *CALIPSO* depolarization measurements were explained through modeling ice crystals with rough surfaces. Best fits to data from Arctic clouds were consistent with deeply rough hexagonal ice crystals (Lampert et al. 2009). Measurements using the polar nephelometer suggested that the surface of Antarctic ice crystals was deeply rough (Shcherbakov et al. 2006).

Uncertain knowledge of the concentrations and shapes of small ice crystals, those with $D < \sim 100\,\mu$m, also hinders progress in understanding the radiative properties of ice clouds. For example, Vogelmann and Ackerman (1995) suggested that radiative fluxes need to be known within about 5% for climate studies, which means that the asymmetry parameter (g) needs to be known within about 2%–5%. Um and McFarquhar (2007) showed that theoretical calculations of g are typically larger than those derived from directional radiation measurements or nephelometer measurements, with assumptions of surface roughness used to reduce the discrepancies (e.g., Yang et al. 2008). However, there is no closure between such radiative and microphysics observations because there are few direct observations of surface roughness at the required scales. While electron microscopy images of pristine crystals grown in laboratories (e.g., Pfalzgraff et al. 2010; Magee et al. 2014) do show some fine surface roughness, it is uncertain how representative this is of atmospheric ice, as such experiments have necessarily been carried out at very low air pressures.

There is also considerable uncertainty in the larger-scale detail of the shapes of small ice crystals, which also affects the scattering properties. For example, columns (Takano and Liou 1995), Chebyshev particles (McFarquhar et al. 2002), droxtals (Yang et al. 2001), Gaussian random spheres (Nousiainen and McFarquhar 2004), budding buckyballs (Um and McFarquhar 2011), and spheres have all been used for representing small particle shapes, with current imaging probes unable to resolve between these shapes. The impacts on calculated single-scattering properties are large enough to appreciably impact g, depending on the crystal shape (McFarquhar et al. 2002). Potential inflation of small particle concentrations due to shattering can also affect g.

5. Radiative properties and feedbacks to climate

Cirrus clouds significantly modify the solar and infrared radiation within the atmosphere. Cirrus clouds reflect a significant part of the incoming solar flux back to space depending on their coverage, position, thickness, and ice crystal size distribution and shape (Yang et al. 2005, 2008, 2015). The reflection of solar radiation results in a cooling effect at the surface and at the top of the atmosphere. However, cirrus clouds also absorb upwelling infrared radiation emitted by Earth's surface and lower atmosphere and emit at much lower temperatures than these, thus reducing the infrared energy escaping the Earth–atmosphere system and eventually lead to warming (Baran 2004). The prevalence of the solar albedo effect versus the infrared greenhouse effect determines the gain or loss of radiative energy, which leads to warming or cooling (Liou 1986).

Ou and Liou (1995) conducted a detailed study on the cirrus cloud climate feedback by studying the radiative behavior of the microphysical properties like ice water path (IWP, the integral of IWC over the vertical extent of the cloud) and the particle effective diameter (D_{eff}, proportional to the IWC/extinction in visible wavelengths). According to this work, both the infrared emissivity and the solar albedo are increasing functions of the IWP and decreasing functions of D_{eff}. Accordingly, as the IWP increases, this results in warming and a positive feedback in the infrared and cooling and, hence, a negative feedback in the visible. Similarly, increasing the effective diameter leads to a positive feedback in the visible and a negative feedback in the infrared. Considering only IWP would result in a net negative feedback, whereas including both IWP and D_{eff} results in a net positive feedback.

Clouds in general and cirrus in particular remain one of the most uncertain components of a general circulation model and pose one of the greatest challenges in predicting the rate and geographical pattern of climate change (IPCC 2007). One reason for this is that cirrus encompass a wide range of optical thicknesses and altitudes. Another reason is that the dynamical processes that generate cirrus, which are different in different geographical areas, are poorly resolved in general circulation models (GCMs). Similarly, the transport of a very small amount of water vapor to and within the upper troposphere, which influences the prediction of cirrus, cannot be vertically resolved in GCMs that typically have 10–20 vertical layers. In the current climate, the global annual mean cirrus cloud radiative effect (the difference is the top-of-the-atmosphere net radiation with and without cirrus clouds) is positive and amounts to $5.7 \, \mathrm{W \, m^{-2}}$, as estimated with the ECHAM6-HAM2 general circulation model (Gasparini and Lohmann 2016). This is larger than estimates from satellite-based studies by Chen et al. (2000) and Hartmann et al. (1992), which obtain the TOA cloud radiative effect of cirrus to be 1.3 and $2.4 \, \mathrm{W \, m^{-2}}$, respectively.

For a doubling of CO_2, the global annual mean surface temperature is projected to increase between 1.5 and 4.5 K (Collins et al. 2013). This warming results from the initial temperature increase due to CO_2 and is enhanced by several positive feedbacks. Of these feedbacks, the cloud feedback has the largest spread between different GCMs and thus is the most uncertain (Vial et al. 2013; Boucher et al. 2013) for the reasons stated above. In addition, because clouds can be smaller than the grid box of a GCM, they need to be parameterized: that is, described in terms of large-scale (grid mean) variables. Therefore GCMs have problems in simulating certain cloud types and cloud microphysical properties. The cloud feedback results in a temperature increase of $0.7 \pm 0.5 \, \mathrm{K}$ (Dufresne and Bony 2008). The contributions to the positive cloud feedback are as follows (Boucher et al. 2013): (i) The rising of high-level clouds implies that the longwave cloud radiative effect increases, which decreases the amount of energy emitted to space. (ii) In a warmer climate the Hadley cell is expected to broaden, which would mean that the storm tracks migrate poleward. This causes low-level clouds to prevail in areas that experience less solar radiation, which decreases their shortwave cloud radiative effect. Zhou et al. (2014) estimated the cloud feedback due to cirrus clouds alone. Because of the rising of high-level clouds, it was found to be positive, with $0.2 \pm 0.2 \, \mathrm{W \, m^{-2} \, K^{-1}}$ (Zhou et al. 2014), and thus it would be a substantial fraction of the cloud feedback if confirmed by other studies.

Better determinations of cirrus optical properties, structure, and vertical and horizontal extent over broad

scales are necessary if we are to improve the projections of the effects of cirrus clouds on climate. Such measurements must be made by satellite, because aircraft, radar, and lidar characterize cloud properties only over very small regions of the planet. However, in order to fully understand the climate impact of cirrus clouds, cirrus clouds must be reliably represented in a physically sound way in climate models. Most climate models now include prognostic equations of the liquid and ice water contents. Two-moment cloud microphysics schemes in addition predict number concentrations of ice crystals. A saturation adjustment, meaning that water vapor in excess of the saturation water vapor will be converted into condensate, is an assumption that is justified in water clouds because of the large number of liquid droplets. This assumption is not justified in cirrus clouds because of the low number of ice crystals that cannot efficiently deplete the gas phase water vapor. Therefore state-of-the-art cirrus schemes abandon the saturation adjustment for cirrus clouds and allow supersaturation with respect to ice (e.g., Lohmann and Kärcher 2002).

The results of GCM simulations indicate that the uncertainty associated with the measurements of small ice crystals may have a deleterious effect on model simulations if current parameterizations of cirrus PSDs are used to constrain the model PSDs. Using different assumed size distributions for small particles, Mitchell et al. (2008) showed that the uncertainties in the concentrations of small ice crystals can cause a 12% difference in cloud ice amount and a 5.5% difference in cirrus cloud coverage globally, largely as a result of the dependence of particle precipitation (sedimentation) rate on the properties of the PSDs, producing an uncertainty in the net cloud forcing in the tropics of $-5\,\mathrm{W\,m^{-2}}$ and in the warming of the upper tropical troposphere of over 3°C. This is comparable to the radiative impacts of CO_2 doubling.

Also, up-to-date climate models that are coupled to aerosol modules consider the competition of homogeneous with heterogeneous ice nucleation and the development of cirrus building on preexisting ice crystals (Kärcher et al. 2006; Penner et al. 2015; note here that preexisting ice represents the category of liquid-origin cirrus introduced in section 3). Heterogeneous ice nucleation—which happens at lower supersaturations than the homogeneous—leads in most cases to cirrus clouds consisting of fewer but larger ice crystals than cirrus that formed homogeneously. This reduces the cirrus optical depth. In addition, the ice crystals sediment faster, further decreasing the optical depth. Heterogeneously formed cirrus clouds thus reflect less solar radiation back to space while at the same time more longwave

radiation is emitted to space. The difference in the net top-of-the-atmosphere radiation amounts to roughly $2\,\mathrm{W\,m^{-2}}$ (Lohmann et al. 2008). Kuebbeler et al. (2014), in another study of the effects of the ice nucleation process, show the difference in cloud properties when only considering homogeneous nucleation and when accounting for the competition between homogeneous and heterogeneous nucleation and growth onto preexisting ice crystals. In the global annual mean, the difference is $1\,\mathrm{W\,m^{-2}}$ in the shortwave cloud forcing (SCF) and $1.5\,\mathrm{W\,m^{-2}}$ in the longwave cloud forcing (LCF). Lohmann et al. (2008) found a much larger influence of the mode of ice nucleation. They compared more extreme scenarios: the difference between considering only heterogeneous nucleation versus only homogeneous nucleation amounts to changes in SCF of $2.7\,\mathrm{W\,m^{-2}}$ and in LCF of $4.7\,\mathrm{W\,m^{-2}}$. However, there is considerable uncertainty in the value of one factor in the mass growth rate of ice crystals, the mass accommodation coefficient. This coefficient, defined as the ratio of the number of molecules incorporated into an ice crystal lattice to the total number of impinging molecules, reflects the still uncertain mechanisms that act at the crystal surface to preclude the successful incorporation of some molecules. To reflect the potential range of uncertainty, they decreased the mass accommodation coefficient from 0.5 to 0.006. This resulted in an increase in the SCF by $14.7\,\mathrm{W\,m^{-2}}$ and LCF by $18.3\,\mathrm{W\,m^{-2}}$.

The difference in the net top-of-the-atmosphere radiation between homogeneous and heterogeneous nucleation led to the proposal by Mitchell and Finnegan (2009) to engineer climate by converting homogeneously formed cirrus clouds into heterogeneously formed cirrus clouds using Bismuth tri-iodide (BiI3), as shown in Fig. 2-14 from Storelvmo et al. (2013).

While Storelvmo et al. (2013) confirmed the negative forcing of $-2\,\mathrm{W\,m^{-2}}$ by cirrus seeding, Penner et al. (2015) and Gasparini and Lohmann (2016) obtained a much smaller negative forcing. They attributed their much smaller forcings to the more dominant role of water vapor uptake by preexisting ice crystals together with a more prominent role of heterogeneous freezing of natural cirrus. The latter is in agreement with the observations by Cziczo et al. (2013).

6. Challenges to our understanding of cirrus formation, evolution, and microphysical properties

According to chapter 7 of the IPCC report (Boucher et al. 2013, p. 583), "Especially for ice clouds, and for interactions between aerosols and clouds, our
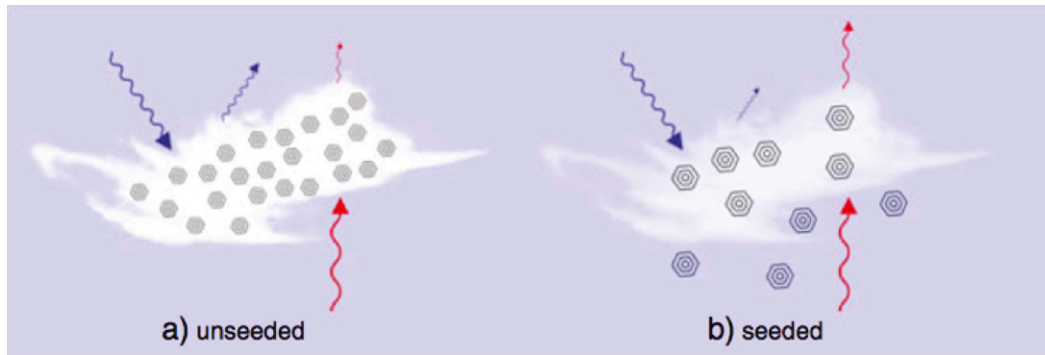
Fig. 2-14. Conceptual schematic of changes in cirrus cloud properties in response to seeding. Red arrows represent longwave (LW) radiation, and blue arrows represent shortwave (SW) radiation. The seeded cirrus clouds on average reflect slightly less SW radiation back to space but also allow more LW radiation to escape to space, and the latter effect dominates. From Storelvmo et al. (2013).

understanding of the basic micro-scale physics is not yet adequate, although it is improving.'' In particular, the complex interactions among cirrus cloud microphysics and dynamics and radiation, sea surface temperature, and climate mean that conclusive results on cirrus cloud–climate interactions will require considerably more knowledge than we currently have. Crucial measurements include size distribution of ice crystals below $100\,\mu$m; scattering behavior of ice crystals as a function of size and habit; cloud radiative properties as a function of temperature, cloud thickness, and height in the atmosphere; and, especially, vertical motion (velocity) fields. There are issues related to sampling of cirrus microphysical properties that need to be considered in future measurements.

The previous sections have summarized many of the observations collected to date both in situ and remotely about the microphysics of cirrus clouds. Those that we believe are reliable include the onset temperature for homogeneous ice nucleation, the direct measurements of the ice water content, the size distributions and shapes of ice particles measured for particle sizes above about 100 or $200\,\mu$m, and the presence of roughness on the surfaces of some of the ice particles. With corrections for shattering and new probe tips, the size distributions measured for particles $20\,\mu$m and above are being derived more accurately than in the past. The more reliable measurements and observations reported to date, including those made prior to awareness by the community of errors produced by shattering of large particles on the leading edges of the particle probes, include the higher moments of the particle size distributions and the size distributions for particles above about $200\,\mu$m. However, there are numerous measurement limitations that need to be overcome if we are to improve our understanding of cirrus physical processes and to more reliably represent them in climate models (see also

Baumgardner et al. 2017, chapter 9). In the future, we need to address the following topics:

1) How can we measure/document the relative importance of homogeneous versus heterogeneous nucleation of cirrus ice crystals?
   • Collect residuals from ice crystals sublimated in the inlet of a counterflow virtual impactor (CVI) probe and measure their chemical composition and size distributions. This is a starting point, but it might be problematic to identify ice crystals that form on preactivated ice nuclei or when there is a mixture of ice particles originating at different times in the life cycle of a cirrus cloud.

2) How are cirrus ice nucleation processes affected by cloud dynamics: gravity waves, shallow and deep convection, radiative cooling at cirrus cloud tops, and turbulence?
   • A considerable amount of ice PSD data are now available for cirrus forming by different dynamical forcing. These data are reasonably reliable if corrections are made to the size distributions by considering particle interarrival times and even more so when imaging probes have Korolev-type tips. A compilation of such data, with this type of study, is needed.

3) What are the size distributions of cirrus particles in the size range of about 1–$20\,\mu$m, where the current generation of probes has a very small sample volume and that volume cannot be reliably specified because the depth of field of focus of the particles is very small (see Korolev et al. 1998)? How do these change for in situ through deep-convectively generated cirrus?
   • This is a very difficult problem to address because particle probes are fundamentally limited by geometrical optics. Holographic probes, now available, can provide the sample volume needed to define

the concentration of small particles, but these instruments are significantly limited by their sampling frequency.

4) How do the properties of cirrus (ice crystal sizes, shapes, scattering properties, mass contents, etc.) vary with the cloud dynamics and geographical location?

   • As in 2), a compilation of existing data is now needed. A field program conducted in the Antarctic to measure cirrus microphysical properties is most urgently needed.

5) There are different approaches to measurement of bulk ice water content (McFarquhar et al. 2017, chapter 11). These instruments measure over different IWC ranges and with differing accuracy. How should these datasets be merged to develop a comprehensive understanding and representation of the IWC?

6) What are the dominant cirrus crystal shapes, and have their scattering properties been reliably represented in climate models and satellite-based retrievals of cirrus cloud microphysical properties?

   • Data from the small ice detector (SID) probes, versions SID-2 and SID-3, are now available to characterize the scattering properties of small cirrus crystals ($<60\,\mu$m) forming in a wide range of environmental conditions and geographic locations. With analysis of these datasets, it will be possible to improve the representation of the scattering properties of ice crystals in climate models and in improving the retrievals of ice cloud properties from active and passive satellite remote sensors.

7) How do cirrus crystal surface properties—especially roughness—influence their scattering properties and, more generally, the radiative properties of cirrus?

   • The conditions that lead to the development of ice crystal roughness or irregularity are still not well understood. Supersaturation has been indicated as one of the main parameters controlling the surface roughness in experiments conducted by Hallett (1987). Dedicated experiments in the Aerosol Interaction and Dynamics in the Atmosphere (AIDA) cloud chamber showed that increasing the peak supersaturation leads to increased roughness (Schnaiter et al. 2016). Also, this was observed following repeated growth/sublimation events (Chou et al. 2014). More laboratory experiments are clearly needed to further understand the processes leading to ice crystal surface roughness.

In future ice cloud measurements, we need to factor in concerns about producing ice particles by the aircraft that we are sampling with, for example, aircraft-produced ice particles. We also need to avoid the contamination of our measurements as a result of aircraft contrails, since these will commonly be produced in circumstances where natural cirrus clouds form and evolve.

REFERENCES

Ackerman, T. P., K. Liou, F. P. J. Valero, and L. Pfister, 1988: Heating rates in tropical anvils. *J. Atmos. Sci.*, **45**, 1606–1623, doi:10.1175/1520-0469(1988)045<1606:HRITA>2.0.CO;2.

American Meteorological Society, 2012: "Cirrus." Glossary of Meteorology. [Available online at http://glossary.ametsoc.org/wiki/Cirrus.]

Auer, A. H., Jr., and D. L. Veal, 1970: The dimensions of ice crystals in natural clouds. *J. Atmos. Sci.*, **27**, 919–926, doi:10.1175/1520-0469(1970)027<0919:TDOICI>2.0.CO;2.

Auriol, F., J.-F. Gayet, G. Febvre, O. Jourdan, L. Labonnotte, and G. Brogniez, 2001: In situ observations of cirrus cloud scattering phase function with 22° and 46° halos: Cloud field study on 19 February 1998. *J. Atmos. Sci.*, **58**, 3376–3390, doi:10.1175/1520-0469(2001)058<3376:ISOOCS>2.0.CO;2.

Bailey, M., and J. Hallett, 2004: Growth rates and habits of ice crystals between −20° and −70°C. *J. Atmos. Sci.*, **61**, 514–544, doi:10.1175/1520-0469(2004)061<0514:GRAHOI>2.0.CO;2.

Baker, B. A., and R. P. Lawson, 2006: Improvement in determination of ice water content from two-dimensional particle imagery. Part I: Image-to-mass relationships. *J. Appl. Meteor. Climatol.*, **45**, 1282–1290, doi:10.1175/JAM2398.1.

Baran, A. J., 2004: On the scattering and absorption properties of cirrus cloud. *J. Quant. Spectrosc. Radiat. Transfer*, **89**, 17–36, doi:10.1016/j.jqsrt.2004.05.008.

——, 2012: From the single-scattering properties of ice crystals to climate prediction: A way forward. *Atmos. Res.*, **112**, 45–69, doi:10.1016/j.atmosres.2012.04.010.

——, P. N. Francis, L.-C. Labonnote, and M. Doutriaux-Boucher, 2001: A scattering phase function for ice cloud: Tests of applicability using aircraft and satellite multi-angle multi-wavelength radiance measurements of cirrus. *Quart. J. Roy. Meteor. Soc.*, **127**, 2395–2416, doi:10.1002/qj.49712757711.

Baum, B. A., P. Yang, A. J. Heymsfield, C. G. Schmitt, Y. Xie, A. Bansemer, Y.-X. Hu, and Z. Zhang, 2011: Improvements in shortwave bulk scattering and absorption models for the remote sensing of ice clouds. *J. Appl. Meteor. Climatol.*, **50**, 1037–1056, doi:10.1175/2010JAMC2608.1.

Baumgardner, D., and Coauthors, 2017: In situ measurement challenges. *Ice Formation and Evolution in Clouds and Precipitation: Measurement and Modeling Challenges*, *Meteor. Monogr.*, No. 58, Amer. Meteor. Soc., doi:10.1175/AMSMONOGRAPHS-D-16-0011.1.

Boucher, O., and Coauthors, 2013: Clouds and aerosols. *Climate Change 2013: The Physical Science Basis,* T. F. Stocker et al., Eds., Cambridge University Press, 571–657. [Available online at http://www.ipcc.ch/pdf/assessment-report/ar5/wg1/WG1AR5_Chapter07_FINAL.pdf.]

Boudala, F. S., A. G. Isaac, Q. Fu, and S. G. Cober, 2002: Parameterization of effective particle sizes for high latitude clouds. *Int. J. Climatol.*, **22**, 1267–1284, doi:10.1002/joc.774.

Chen, T., W. B. Rossow, and Y. C. Zhang, 2000: Radiative effects of cloud-type variations. *J. Climate*, **13**, 264–286, doi:10.1175/1520-0442(2000)013<0264:REOCTV>2.0.CO;2.

Chou, C., and Coauthors, 2014: Growth and sublimation of rough ice crystals in a flow diffusion chamber. *Extended Abstracts, 45th Annual Conf. of the British Association Crystal Growth*, Leeds, United Kingdom, British Association for Crystal Growth, 704.

Cole, B. H., P. Yang, B. A. Baum, J. Riedi, L. C. Labonnote, F. Thieuleux, and S. Platnick, 2013: Comparison of PARASOL observations with polarized reflectances simulated using different ice habit mixtures. *J. Appl. Meteor. Climatol.*, **52**, 186–196, doi:10.1175/JAMC-D-12-097.1.

Collins, M., and Coauthors, 2013: Long-term climate change: Projections, commitments and irreversibility. *Climate Change 2013: The Physical Science Basis,* T. F. Stocker et al., Eds., Cambridge University Press, 1029–1136, doi:10.1017/CBO9781107415324.024.

Connolly, P. J., M. J. Flynn, Z. Ulanowski, T. W. Choularton, M. W. Gallagher, and K. N. Bower, 2007: Calibration of 2 D imaging probes using calibration beads and ice crystal analogues. *J. Atmos. Oceanic Technol.*, **24**, 1860–1879, doi:10.1175/JTECH2096.1.

Cziczo, D. J., and Coauthors, 2013: Clarifying the dominant sources and mechanisms of cirrus cloud formation. *Science*, **340**, 1320–1324, doi:10.1126/science.1234145.

——, L. Ladino-Moreno, Y. Boose, Z. Kanji, P. Kupiszewski, S. Lance, S. Mertes, and H. Wex, 2017: Measurements of ice nucleating particles and ice residuals. *Ice Formation and Evolution in Clouds and Precipitation: Measurement and Modeling Challenges*, *Meteor. Monogr.*, No. 58, Amer. Meteor. Soc., doi:10.1175/AMSMONOGRAPHS-D-16-0008.1.

Davis, C. I., 1974: The ice-nucleating characteristics of various AgI aerosols. Ph.D. dissertation, University of Wyoming, 267 pp.

Delanoë, J., and R. J. Hogan, 2010: Combined *CloudSat–CALIPSO–MODIS* retrievals of the properties of ice clouds. *J. Geophys. Res.*, **115**, D00H29, doi:10.1029/2009JD012346.

——, A. Protat, J. Testud, D. Bouniol, A. J. Heymsfield, A. Bansemer, P. R. A. Brown, and R. M. Forbes, 2005: Statistical properties of the normalized ice particle size distribution. *J. Geophys. Res.*, **110**, D10201, doi:10.1029/2004JD005405.

DeMott, P. J., K. Sassen, M. R. Poellot, D. Baumgardner, D. C. Rogers, S. D. Brooks, A. J. Prenni, and S. M. Kreidenweis, 2003: African dust aerosols as atmospheric ice nuclei. *Geophys. Res. Lett.*, **30**, 1732, doi:10.1029/2003GL017410.

——, and Coauthors, 2010: Predicting global atmospheric ice nuclei distributions and their impacts on climate. *Proc. Natl. Acad. Sci. USA*, **107**, doi:10.1073/pnas.0910818107.

Deng, M., G. G. Mace, Z. Wang, and R. P. Lawson, 2013: Evaluation of several A-Train ice cloud retrieval products with in situ measurements collected during the SPARTICUS campaign. *J. Appl. Meteor. Climatol.*, **52**, 1014–1030, doi:10.1175/JAMC-D-12-054.1.

——, ——, ——, and E. Berry, 2015: *CloudSat* 2C-ICE product update with a new Z_e parameterization in lidar-only region. *J. Geophys. Res.*, **120**, 12 198–12 208, doi:10.1002/2015JD023600.

Dufresne, J.-L., and S. Bony, 2008: An assessment of the primary sources of spread of global warming estimates from coupled atmosphere–ocean models. *J. Climate*, **21**, 5135–5144, doi:10.1175/2008JCLI2239.1.

Durran, D. R., T. Dinh, M. Ammerman, and T. Ackerman, 2009: The mesoscale dynamics of thin tropical tropopause cirrus. *J. Atmos. Sci.*, **66**, 2859–2873, doi:10.1175/2009JAS3046.1.

Field, P. R., and A. J. Heymsfield, 2003: Aggregation and scaling of ice crystal distributions. *J. Atmos. Sci.*, **60**, 544–560, doi:10.1175/1520-0469(2003)060<0544:AASOIC>2.0.CO;2.

Field, R. P., A. J. Heymsfield, and A. Bansemer, 2006: Shattering and particle interarrival times measured by optical array probes in ice clouds. *J. Atmos. Oceanic Technol.*, **23**, 1357–1370, doi:10.1175/JTECH1922.1.

——, ——, and ——, 2007: Snow size distribution parameterization for midlatitude and tropical ice clouds. *J. Atmos. Sci.*, **64**, 4346–4365, doi:10.1175/2007JAS2344.1.

Foot, J. S., 1988: Some observations of the optical properties of clouds. II: Cirrus. *Quart. J. Roy. Meteor. Soc.*, **114**, 145–164, doi:10.1002/qj.49711447908.

Frey, W., and Coauthors, 2011: In situ measurements of tropical cloud properties in the West African Monsoon: Upper tropospheric ice clouds, Mesoscale Convective System outflow, and subvisual cirrus. *Atmos. Chem. Phys.*, **11**, 5569–5590, doi:10.5194/acp-11-5569-2011.

Fu, Q., 2007: A new parameterization of an asymmetry factor of cirrus clouds for climate models. *J. Atmos. Sci.*, **64**, 4140–4150, doi:10.1175/2007JAS2289.1.

Fusina, F., and P. Spichtinger, 2010: Cirrus clouds triggered by radiation, a multiscale phenomenon. *Atmos. Chem. Phys.*, **10**, 5179–5190, doi:10.5194/acp-10-5179-2010.

Gallagher, M. W., and Coauthors, 2005: An overview of the microphysical structure of cirrus clouds observed during EMERALD-I. *Quart. J. Roy. Meteor. Soc.*, **131**, 1143–1169, doi:10.1256/qj.03.138.

Garrett, T. J., 2008: *Observational quantification of the optical properties of cirrus cloud*. Light Scattering Reviews 3, A. A. Kokhanovsky, Ed., Springer, 3–26, doi:10.1007/978-3-540-48546-9_1.

——, and Coauthors 2005: Evolution of a Florida cirrus anvil. *J. Atmos. Sci.*, **62**, 2352–2372, doi:10.1175/JAS3495.1.

Gasparini, B., and U. Lohmann, 2016: Why cirrus cloud seeding cannot substantially cool the planet. *J. Geophys. Res. Atmos.*, **121**, 4877–4893, doi:10.1002/2015JD024666.

Gayet, J.-F., G. Mioche, V. Shcherbakov, C. Gourbeyre, R. Busen, and A. Minikin, 2011: Optical properties of pristine ice crystals in mid-latitude cirrus clouds: A case study during CIRCLE-2 experiment. *Atmos. Chem. Phys.*, **11**, 2537–2544, doi:10.5194/acp-11-2537-2011.

Gunn, K. L. S., and J. S. Marshall, 1958: The distribution with size of aggregate snowflakes. *J. Meteor.*, **15**, 452–461, doi:10.1175/1520-0469(1958)015<0452:TDWSOA>2.0.CO;2.

Hahn, C. J., and S. G. Warren, 2007: A gridded climatology of clouds over land (1971–96) and ocean (1954–97) from surface observations worldwide. Carbon Dioxide Information Analysis Center Numeric Data Package NDP-026E, 71 pp.

Hallett, J., 1987: Faceted snow crystals. *J. Opt. Soc. Amer.*, **4A**, 581–588, doi:10.1364/JOSAA.4.000581.

Hartmann, D. L., M. E. Ockert-Bell, and M. L. Michelsen, 1992: The effect of cloud type on earth's energy balance: Global analysis. *J. Climate*, **5**, 1281–1304, doi:10.1175/1520-0442(1992)005<1281:TEOCTO>2.0.CO;2.

Heymsfield, A. J., 1975a: Cirrus uncinus generating cells and the evolution of cirriform clouds. Part I: Aircraft observations of the growth of the ice phase. *J. Atmos. Sci.*, **32**, 799–808, doi:10.1175/1520-0469(1975)032<0799:CUGCAT>2.0.CO;2.

——, 1975b: Cirrus uncinus generating cells and the evolution of cirriform clouds. Part II: The structure and circulations of the cirrus uncinus generating head. *J. Atmos. Sci.*, **32**, 809–819, doi:10.1175/1520-0469(1975)032<0809:CUGCAT>2.0.CO;2.

——, 1975c: Cirrus uncinus generating cells and the evolution of cirriform clouds. Part III: Numerical computations of the growth of the ice phase. *J. Atmos. Sci.*, **32**, 820–830, doi:10.1175/1520-0469(1975)032<0820:CUGCAT>2.0.CO;2.

——, 1977: Precipitation development in stratiform ice clouds: A microphysical and dynamical study. *J. Atmos. Sci.*, **34**, 367–381, doi:10.1175/1520-0469(1977)034<0367:PDISIC>2.0.CO;2.

——, and C. M. R. Platt, 1984: A parameterization of the particle size spectrum of ice clouds in terms of ambient temperature and their ice water content. *J. Atmos. Sci.*, **41**, 846–855, doi:10.1175/1520-0469(1984)041<0846:APOTPS>2.0.CO;2.

——, and L. M. Miloshevich, 1993: Homogeneous ice nucleation and supercooled liquid water in orographic wave clouds. *J. Atmos. Sci.*, **50**, 2335–2353, doi:10.1175/1520-0469(1993)050<2335:HINASL>2.0.CO;2.

——, and ——, 1995: Relative humidity and temperature influences on cirrus formation and evolution: Observations from wave clouds and FIRE II. *J. Atmos. Sci.*, **52**, 4302–4326, doi:10.1175/1520-0469(1995)052<4302:RHATIO>2.0.CO;2.

——, and G. M. McFarquhar, 2002: Mid-latitude and tropical cirrus: Microphysical properties. *Cirrus*, D. Lynch et al., Ed., Oxford University Press, 78–101.

——, A. Bansemer, P. R. Field, S. L. Durden, J. Stith, J. E. Dye, and W. Hall, 2002: Observations and parameterizations of particle size distributions in deep tropical cirrus and stratiform clouds: Results from in situ observations in TRMM field campaigns. *J. Atmos. Sci.*, **59**, 3457–3491, doi:10.1175/1520-0469(2002)059<3457:OAPOPS>2.0.CO;2.

——, ——, G. Heymsfield, and A. O. Fierro, 2009: Microphysics of maritime tropical convective updrafts at temperatures from −20° to −60°C. *J. Atmos. Sci.*, **66**, 3530–3562, doi:10.1175/2009JAS3107.1.

——, C. Schmitt, and A. Bansemer, 2013: Ice cloud particle size distributions and pressure-dependent terminal velocities from in situ observations at temperatures from 0° to −86°C. *J. Atmos. Sci.*, **70**, 4123–4154, doi:10.1175/JAS-D-12-0124.1.

——, M. Krämer, N. B. Wood, A. Gettelman, P. R. Field, and G. Liu, 2017: Dependence of the ice water content and snowfall rate on temperature, globally: Comparison of in situ observations, satellite active remote sensing retrievals, and global climate model simulations. *J. Appl. Meteor. Climatol.*, doi:10.1175/JAMC-D-16-0230.1, in press.

Heymsfield, G. M., L. Tian, A. J. Heymsfield, L. Li, and S. Guimond, 2010: Characteristics of deep tropical and subtropical convection from nadir-viewing high-altitude airborne Doppler radar. *J. Atmos. Sci.*, **67**, 285–308, doi:10.1175/2009JAS3132.1.

Hobbs, P. V., S. Chang, and J. D. Locatelli, 1974: The dimensions and aggregation of ice crystals in natural clouds. *J. Geophys. Res.*, **79**, 2199–2206, doi:10.1029/JC079i015p02199.

Huschke, R. E., 1970: *Glossary of Meteorology*. Amer. Meteor. Soc., 638 pp.

IPCC, 2007: *Climate Change 2007: The Physical Science Basis*. Cambridge University Press, 996 pp.

Ivanova, D. C., D. L. Mitchell, W. Patrick Arnott, and M. Poellot, 2001: A GCM parameterization for bimodal size spectra and ice mass removal rates in mid-latitude cirrus clouds. *Atmos. Res.*, **59–60**, 89–113, doi:10.1016/S0169-8095(01)00111-9.

Jackson, R. C., and G. M. McFarquhar, 2014: An assessment of the impact of anti-shattering tips and artifact removal techniques on bulk cloud ice microphysical and optical properties measured by the 2D cloud probe. *J. Atmos. Oceanic Technol.*, **31**, 2131–2144, doi:10.1175/JTECH-D-14-00018.1.

——, ——, J. Stith, M. Beals, R. Shaw, J. Jensen, J. Fugal, and A. Korolev, 2014: An assessment of the impact of anti-shattering tips and artifact removal techniques on cloud ice size distributions measured by the 2D cloud probe. *J. Atmos. Oceanic Technol.*, **31**, 2567–2590, doi:10.1175/JTECH-D-13-00239.1.

——, ——, A. Fridlind, and R. Atlas, 2015: The dependence of cirrus gamma size distributions expressed as volumes in N_0–λ–μ phase space and bulk cloud properties on environmental conditions: Results from the Small Ice Particles in Cirrus Experiment (SPARTICUS). *J. Geophys. Res.*, **120**, 10 351–10 377, doi:10.1002/2015JD023492.

Jensen, E. J., O. B. Toon, H. B. Selkirk, J. D. Spinhirne, and M. R. Schoeberl, 1996: On the formation and persistence of subvisible cirrus clouds near the tropical tropopause. *J. Geophys. Res.*, **101**, 21 361–21 375, doi:10.1029/95JD03575.

Joos, H., P. Spichtinger, P. Reutter, and F. Fusina, 2014: Influence of heterogeneous freezing on the microphysical and radiative properties of orographic cirrus clouds. *Atmos. Chem. Phys.*, **14**, 6835–6852, doi:10.5194/acp-14-6835-2014.

Kanji, Z. A., L. A. Ladino, H. Wex, Y. Boose, M. Burkert-Kohn, D. Cziczo, and M. Krämer, 2017: Heterogeneous ice nucleation. *Ice Formation and Evolution in Clouds and Precipitation: Measurement and Modeling Challenges*, Meteor. Monogr., No. 58, Amer. Meteor. Soc., doi:10.1175/AMSMONOGRAPHS-D-16-0006.1.

Kärcher, B., and U. Lohmann, 2002: A parameterization of cirrus cloud formation: Homogeneous freezing of supercooled aerosols. *J. Geophys. Res.*, **107**, AAC 4-1–AAC 4-10, doi:10.1029/2001JD000470.

——, and ——, 2003: A parameterization of cirrus cloud formation: Heterogeneous freezing. *J. Geophys. Res.*, **108**, 4402, doi:10.1029/2002JD003220.

——, J. Hendricks, and U. Lohmann, 2006: Physically based parameterization of cirrus cloud formation for use in global atmospheric models. *J. Geophys. Res.*, **111**, D01205, doi:10.1029/2005JD006219.

Kay, J. E., M. Baker, and D. Hegg, 2006: Microphysical and dynamical controls on cirrus cloud optical depth distributions. *J. Geophys. Res.*, **111**, D24205, doi:10.1029/2005JD006916.

Khvorostyanov, V. I., and K. Sassen, 1998: Cirrus cloud simulation using explicit microphysics and radiation. Part II: Microphysics, vapor and ice mass budgets, and optical and radiative properties. *J. Atmos. Sci.*, **55**, 1822–1845, doi:10.1175/1520-0469(1998)055<1822:CCSUEM>2.0.CO;2.

Koop, T., B. P. Luo, A. Tsias, and T. Peter, 2000: Water activity as the determinant for homogeneous ice nucleation in aqueous solutions. *Nature*, **406**, 611–614, doi:10.1038/35020537.

Korolev, A. V., J. W. Strapp, and G. A. Isaac, 1998: Evaluation of the accuracy of PMS optical array probes. *J. Atmos. Oceanic Technol.*, **15**, 708–720, doi:10.1175/1520-0426(1998)015<0708:EOTAOP>2.0.CO;2.

——, G. A. Isaac, and J. Hallett, 1999: Ice particle habits in Arctic clouds. *Geophys. Res. Lett.*, **26**, 1299–1302, doi:10.1029/1999GL900232.

——, ——, I. P. Mazin, and H. Barker, 2001: Microphysical properties of continental clouds from in-situ measurements. *Quart. J. Roy. Meteor. Soc.*, **127**, 2117–2151, doi:10.1002/qj.49712757614.

——, E. F. Emery, J. W. Strapp, S. G. Cober, G. A. Isaac, M. Wasey, and D. Marcotte, 2011: Small ice particles in tropospheric clouds: Fact or artifact? *Bull. Amer. Meteor. Soc.*, **92**, 967–973, doi:10.1175/2010BAMS3141.1.

——, J. W. Strapp, G. A. Isaac, and E. Emery, 2013: Improved airborne hot-wire measurements of ice water content in clouds. *J. Atmos. Oceanic Technol.*, **30**, 2121–2131, doi:10.1175/JTECH-D-13-00007.1.

Kox, S., L. Bugliaro, and A. Ostler, 2014: Retrieval of cirrus cloud optical thickness and top altitude from geostationary remote sensing. *Atmos. Meas. Tech.*, **7**, 3233–3246, doi:10.5194/amt-7-3233-2014.

Krämer, M., and Coauthors, 2009: Ice supersaturations and cirrus cloud crystal numbers. *Atmos. Chem. Phys.*, **9**, 3505–3522, doi:10.5194/acp-9-3505-2009.

——, and Coauthors, 2016: A microphysics guide to cirrus clouds. Part I: Cirrus types. *Atmos. Chem. Phys.*, **16**, 3463–3483, doi:10.5194/acp-16-3463-2016.

Kuebbeler, M., U. Lohmann, J. Hendricks, and B. Kärcher, 2014: Dust ice nuclei effects on cirrus clouds. *Atmos. Chem. Phys.*, **14**, 3027–3046, doi:10.5194/acp-14-3027-2014.

Lampert, A., and Coauthors, 2009: Microphysical and radiative characterization of a subvisible midlevel Arctic ice cloud by airborne observations—A case study. *Atmos. Chem. Phys.*, **9**, 2647–2661, doi:10.5194/acp-9-2647-2009.

Lawson, R. P., E. J. Jensen, D. L. Mitchell, B. Baker, Q. Mo, and B. Pilson, 2010: Microphysical and radiative properties of tropical clouds investigated in TC4 and NAMMA. *J. Geophys. Res.*, **115**, D00J08, doi:10.1029/2009JD013017.

Lilly, D., 1988: Cirrus outflow dynamics. *J. Atmos. Sci.*, **45**, 1594–1605, doi:10.1175/1520-0469(1988)045<1594:COD>2.0.CO;2.

Liou, K. N., 1986: Influence of cirrus clouds on weather and climate processes: A global perspective. *Mon. Wea. Rev.*, **114**, 1167–1199, doi:10.1175/1520-0493(1986)114<1167:IOCCOW>2.0.CO;2.

Lohmann, U., and B. Kärcher, 2002: First interactive simulations of cirrus clouds formed by homogeneous freezing in the ECHAM general circulation model. *J. Geophys. Res.*, **107**, 4105–4118, doi:10.1029/2001JD000767.

——, P. Spichtinger, S. Jess, T. Peter, and H. Smit, 2008: Cirrus cloud formation and ice supersaturated regions in a global climate model. *Environ. Res. Lett.*, **3**, 045022, doi:10.1088/1748-9326/3/4/045022.

Luebke, A. E., L. M. Avallone, C. Schiller, J. Meyer, C. Rolf, and M. Krämer, 2013: Ice water content of Arctic, midlatitude, and tropical cirrus—Part 2: Extension of the database and new statistical analysis. *Atmos. Chem. Phys.*, **13**, 6447–6459, doi:10.5194/acp-13-6447-2013.

——, and Coauthors, 2016: The origin of midlatitude ice clouds and the resulting influence on their microphysical properties. *Atmos. Chem. Phys.*, **16**, 5793–5809, doi:10.5194/acp-16-5793-2016.

Lynch, D. K., K. Sassen, D. O'C. Starr, and G. Stephens, Eds., 2002: *Cirrus*, Oxford University Press, 504 pp.

Mace, G. G., and Q. Zhang, 2014: The *CloudSat* radar–lidar geometrical profile product (RL-GeoProf): Updates, improvements, and selected results. *J. Geophys. Res.*, 9441–9462, doi:10.1002/2013JD021374.

——, ——, M. Vaughn, R. Marchand, G. Stephens, C. Trepte, and D. Winker, 2009: A description of hydrometeor layer occurrence statistics derived from the first year of merged *CloudSat* and *CALIPSO* data. *J. Geophys. Res.*, **114**, D00A26, doi:10.1029/2007JD009755.

Macke, A., J. Mueller, and E. Raschke, 1996: Single scattering properties of atmospheric ice crystals. *J. Atmos. Sci.*, **53**, 2813–2825, doi:10.1175/1520-0469(1996)053<2813:SSPOAI>2.0.CO;2.

Magee, N. B., A. Miller, M. Amaral, and A. Cumiskey, 2014: Mesoscopic surface roughness of ice crystals pervasive across a wide range of ice crystal conditions. *Atmos. Chem. Phys.*, **14**, 12 357–12 371, doi:10.5194/acp-14-12357-2014.

McFarquhar, G. M., and A. J. Heymsfield, 1996: Microphysical characteristics of three cirrus anvils sampled during the Central Equatorial Pacific Experiment (CEPEX). *J. Atmos. Sci.*, **53**, 2401–2423, doi:10.1175/1520-0469(1996)053<2401:MCOTAS>2.0.CO;2.

——, and ——, 1997: Parameterization of tropical cirrus ice crystal size distributions and implications for radiative transfer: Results from CEPEX. *J. Atmos. Sci.*, **54**, 2187–2200, doi:10.1175/1520-0469(1997)054<2187:POTCIC>2.0.CO;2.

——, and ——, 1998: The definition and significance of an effective radius for ice clouds. *J. Atmos. Sci.*, **55**, 2039–2052, doi:10.1175/1520-0469(1998)055<2039:TDASOA>2.0.CO;2.

——, and R. A. Black, 2004: Observations of particle size and phase in tropical cyclones: Implications for mesoscale modeling of microphysical processes. *J. Atmos. Sci.*, **61**, 422–439, doi:10.1175/1520-0469(2004)061<0422:OOPSAP>2.0.CO;2.

——, A. J. Heymsfield, J. Spinhirne, and B. Hart, 2000: Thin and subvisual tropopause tropical cirrus: Observations and radiative impacts. *J. Atmos. Sci.*, **57**, 1841–1853, doi:10.1175/1520-0469(2000)057<1841:TASTTC>2.0.CO;2.

——, P. Yang, A. Macke, and A. J. Baran, 2002: A new parameterization of single scattering solar radiative properties for tropical anvils using observed ice crystal size and shape distributions. *J. Atmos. Sci.*, **59**, 2458–2478, doi:10.1175/1520-0469(2002)059<2458:ANPOSS>2.0.CO;2.

——, J. Um, M. Freer, D. Baumgardner, G. L. Kok, and G. Mace, 2007a: The importance of small ice crystals to cirrus properties: Observations from the Tropical Western Pacific International Cloud Experiment (TWP-ICE). *Geophys. Res. Lett.*, **34**, L13803, doi:10.1029/2007GL029865.

——, M. S. Timlin, R. M. Rauber, B. F. Jewett, J. A. Grim, and D. P. Jorgensen, 2007b: Vertical variability of cloud hydrometeors in the stratiform region of mesoscale convective systems and bow echoes. *Mon. Wea. Rev.*, **135**, 3405–3428, doi:10.1175/MWR3444.1.

——, T.-L. Hsieh, M. Freer, J. Mascio, and B. F. Jewett, 2015: The characterization of ice hydrometeor gamma size distributions as volumes in N_0–λ–μ phase space: Implications for microphysical process modeling. *J. Atmos. Sci.*, **72**, 892–909, doi:10.1175/JAS-D-14-0011.1.

——, and Coauthors, 2017: Data analysis, interpretation, and presentation of in situ measurements. *Ice Formation and Evolution in Clouds and Precipitation: Measurement and Modeling Challenges*, *Meteor. Monogr.*, No. 58, Amer. Meteor. Soc., doi:10.1175/AMSMONOGRAPHS-D-16-0007.1.

Miloshevich, L. M., and A. J. Heymsfield, 1997: A balloon-borne continuous cloud particle replicator for measuring vertical profiles of cloud microphysical properties: Instrument design, performance, and collection efficiency analysis. *J. Atmos. Oceanic Technol.*, **14**, 753–768, doi:10.1175/1520-0426(1997)014<0753:ABBCCP>2.0.CO;2.

Mishchenko, M. I., and A. Macke, 1999: How big should hexagonal ice crystals be to produce halos? *Appl. Opt.*, **38**, 1626–1629, doi:10.1364/AO.38.001626.

Mitchell, D. L., and W. P. Arnott, 1994: A model predicting the evolution of ice particle size spectra and radiative properties of cirrus clouds. Part II: Dependence of absorption and extinction on ice crystal morphology. *J. Atmos. Sci.*, **51**, 817–832, doi:10.1175/1520-0469(1994)051<0817:AMPTEO>2.0.CO;2.

——, and W. Finnegan, 2009: Modification of cirrus clouds to reduce global warming. *Environ. Res. Lett.*, **4**, 045102, doi:10.1088/1748-9326/4/4/045102.

——, S. K. Chai, Y. Liu, A. J. Heymsfield, and Y. Dong, 1996: Modeling cirrus clouds. Part I: Treatment of bimodal size spectra and case study analysis. *J. Atmos. Sci.*, **53**, 2952–2966, doi:10.1175/1520-0469(1996)053<2952:MCCPIT>2.0.CO;2.

——, R. Phillip, D. Ivanova, G. M. McFarquhar, and T. Nousiainen, 2008: Impacts of small ice crystal assumption on ice sedimentation rates in cirrus clouds and GCM simulations. *Geophys. Res. Lett.*, **35**, L09806, doi:10.1029/2008GL033552.

——, R. P. d'Entremont, and R. P. Lawson, 2010: Inferring cirrus size distributions through satellite remote sensing and microphysical databases. *J. Atmos. Sci.*, **67**, 1106–1125, doi:10.1175/2009JAS3150.1.

Muhlbauer, A., T. P. Ackerman, J. M. Comstock, G. S. Diskin, S. M. Evans, R. P. Lawson, and R. T. Marchand, 2014: Impact of large-scale dynamics on the microphysical properties of midlatitude cirrus. *J. Geophys. Res.*, **119**, 3976–3996, doi:10.1002/2013JD020035.

Nazaryan, H., M. P. McCormick, and W. P. Menzel, 2008: Global characterization of cirrus clouds using CALIPSO data. *J. Geophys. Res.*, **113**, D16211, doi:10.1029/2007JD009481.

Nelson, J., and C. Knight, 1998: Snow crystal habit changes explained by layer nucleation. *J. Atmos. Sci.*, **55**, 1452–1465, doi:10.1175/1520-0469(1998)055<1452:SCHCEB>2.0.CO;2.

Nousiainen, T., and G. M. McFarquhar, 2004: Radiative properties of small quasi-spherical ice crystals. *J. Atmos. Sci.*, **61**, 2229–2248, doi:10.1175/1520-0469(2004)061<2229:LSBQIC>2.0.CO;2.

Ou, S. C., and K. N. Liou, 1995: Ice microphysics and climatic temperature feedback. *Atmos. Res.*, **35**, 127–138, doi:10.1016/0169-8095(94)00014-5.

Penner, J. E., C. Zhou, and X. Liu, 2015: Can cirrus cloud seeding be used for geoengineering? *Geophys. Res. Lett.*, **43**, 8775–8782, doi:10.1002/2015GL065992.

Pfalzgraff, W. C., R. M. Hulscher, and S. P. Neshyba, 2010: Scanning electron microscopy and molecular dynamics of surfaces of growing and ablating hexagonal ice crystals. *Atmos. Chem. Phys.*, **10**, 2927–2935, doi:10.5194/acp-10-2927-2010.

Pruppacher, H. R., and J. D. Klett, 1997: *Microphysics of Clouds and Precipitation*, 2nd ed. Atmospheric and Oceanographic Sciences Library, Vol. 18, Kluwer Academic Publishers, 954 pp., doi:10.1007/978-0-306-48100-0.

Ramanathan, V., and W. Collins, 1991: Thermodynamic regulation of ocean warming by cirrus clouds deduced from observations of the 1987 El Niño. *Nature*, **351**, 27–32, doi:10.1038/351027a0.

Ramaswamy, V., and A. Detwiler, 1986: Interdependence of radiation and microphysics in cirrus clouds. *J. Atmos. Sci.*, **43**, 2289–2301, doi:10.1175/1520-0469(1986)043<2289:IORAMI>2.0.CO;2.

Riese, M., F. Ploeger, A. Rap, B. Vogel, P. Konopka, M. Dameris, and P. Forster, 2012: Impact of uncertainties in atmospheric mixing on simulated UTLS composition and related radiative effects. *J. Geophys. Res.*, **117**, D16305, doi:10.1029/2012JD017751.

Sassen, K., Z. Wang, V. I. Khvorostyanov, G. L. Stephens, and A. Benedetti, 2002: Cirrus cloud ice water content radar algorithm evaluation using an explicit cloud microphysical model. *J. Appl. Meteor.*, **41**, 620–628, doi:10.1175/1520-0450(2002)041<0620:CCIWCR>2.0.CO;2.

——, ——, and D. Liu, 2008: Global distribution of cirrus clouds from CloudSat/Cloud–Aerosol Lidar and Infrared Pathfinder Satellite Observations (CALIPSO) measurements. *J. Geophys. Res.*, **113**, D00A12, doi:10.1029/2008JD009972.

——, ——, and ——, 2009: Cirrus clouds and deep convection in the tropics: Insights from CALIPSO and CloudSat. *J. Geophys. Res.*, **114**, D00H06, doi:10.1029/2009JD011916.

Schiller, C., M. Krämer, A. Afchine, N. Spelten, and N. Sitnikov, 2008: Ice water content in Arctic, midlatitude, and tropical cirrus. *J. Geophys. Res.*, **113**, D24208, doi:10.1029/2008JD010342.

Schnaiter, M., and Coauthors, 2016: Cloud chamber experiments on the origin of ice crystal complexity in cirrus clouds. *Atmos. Chem. Phys.*, **16**, 5091–5110, doi:10.5194/acp-16-5091-2016.

Shcherbakov, V., J. F. Gayet, O. Jourdan, J. Ström, and A. Minikin, 2006: Light scattering by single ice crystals of cirrus clouds. *Geophys. Res. Lett.*, **33**, L15809, doi:10.1029/2006GL026055.

Spichtinger, P., and D. J. Cziczo, 2010: Impact of heterogeneous ice nuclei on homogeneous freezing events in cirrus clouds. *J. Geophys. Res.*, **115**, D14208, doi:10.1029/2009JD012168.

Starr, D. O'C., and S. K. Cox, 1985: Cirrus clouds. Part II: Numerical experiment on the formation and maintenance of cirrus. *J. Atmos. Sci.*, **42**, 2682–2694, doi:10.1175/1520-0469(1985)042<2682:CCPINE>2.0.CO;2.

Stephens, G. L., and Coauthors, 2002: The CloudSat mission and the A-Train: A new dimension to space-based observations of clouds and precipitation. *Bull. Amer. Meteor. Soc.*, **83**, 1771–1790, doi:10.1175/BAMS-83-12-1771.

Storelvmo, T., J. E. Kristjansson, H. Muri, M. A. Pfeffer, D. Barahona, and A. Nenes, 2013: Cirrus cloud seeding has potential to cool climate. *Geophys. Res. Lett.*, **40**, 178–182, doi:10.1029/2012GL054201.

Takano, Y., and K. N. Liou, 1989: Solar radiative transfer in cirrus clouds. Part I: Single-scattering and optical properties of hexagonal ice crystals. *J. Atmos. Sci.*, **46**, 3–19, doi:10.1175/1520-0469(1989)046<0003:SRTICC>2.0.CO;2.

——, and ——, 1995: Radiative transfer in cirrus clouds. Part III: Light scattering by irregular ice crystals. *J. Atmos. Sci.*, **52**, 818–837, doi:10.1175/1520-0469(1995)052<0818:RTICCP>2.0.CO;2.

Ulanowski, Z., 2005: Ice analog halos. *Appl. Opt.*, **44**, 5754–5758, doi:10.1364/AO.44.005754.

——, P. Connolly, M. Flynn, M. Gallagher, A. J. M. Clarke, and E. Hesse, 2004: Using ice crystal analogues to validate cloud ice parameter retrievals from the CPI ice spectrometer data. *Proc. 14th Int. Conf. on Clouds & Precipitation*, Bologna, Italy, International Commission on Clouds and Precipitation, 1175–1178.

——, E. Hesse, P. H. Kaye, and A. J. Baran, 2006: Light scattering by complex ice-analogue crystals. *J. Quant. Spectrosc. Radiat. Transfer*, **100**, 382–392, doi:10.1016/j.jqsrt.2005.11.052.

Um, J. S., and G. M. McFarquhar, 2007: Single-scattering properties of aggregates of bullet rosettes in cirrus. *J. Appl. Meteor. Climatol.*, **46**, 757–775, doi:10.1175/JAM2501.1.

——, and ——, 2009: Single-scattering properties of aggregates of plates from TWP-ICE. *Quart. J. Roy. Meteor. Soc.*, **135**, 291–304, doi:10.1002/qj.378.

——, and ——, 2011: Dependence of the single-scattering properties of small ice crystals on idealized shape models. *Atmos. Chem. Phys.*, **11**, 3159–3171, doi:10:5914/acp-11-3159-2011.

——, and ——, 2015: Formation of atmospheric halos and applicability of geometric optics for calculating single-scattering

properties of hexagonal ice crystals: Impacts of aspect ratio and crystal size. *J. Quant. Spectrosc. Radiat. Transfer*, **165**, 134–152, doi:10.1016/j.jqsrt.2015.07.001.

Um, J., G. M. McFarquhar, Y. P. Hong, S.-S. Lee, C. H. Jung, R. P. Lawson, and Q. Mo, 2015: Dimensions and aspect ratios of natural ice crystals. *Atmos. Chem. Phys.*, **15**, 3933–3956, doi:10.5194/acp-15-3933-2015.

Vial, J., J.-L. Dufresne, and S. Bony, 2013: On the interpretation of inter-model spread in CMIP5 climate sensitivity estimates. *Climate Dyn.*, **41**, 3339–3362, doi:10.1007/s00382-013-1725-9.

Vogelmann, A. M., and T. P. Ackerman, 1995: Relating cirrus cloud radiative properties to observed fluxes—A critical assessment. *J. Atmos. Sci.*, **52**, 4285–4301, doi:10.1175/1520-0469(1995)052<4285:RCCPTO>2.0.CO;2.

Wagner, R., A. Kiselev, O. Moehler, H. Saathoff, and I. Steinke, 2016: Pre-activation of ice-nucleating particles by the pore condensation and freezing mechanism. *Atmos. Chem. Phys.*, **16**, 2025–2042, doi:10.5194/acp-16-2025-2016.

Weickman, H. K., 1948: *Die Eisphase in der Atmosphare*. Royal Aircraft Establishment, 96 pp.

Winker, D. M., M. A. Vaughan, A. H. Omar, Y. Hu, K. A. Powell, Z. Liu, W. H. Hunt, and S. A. Young, 2009: Overview of the *CALIPSO* mission and CALIOP data processing algorithms. *J. Atmos. Oceanic Technol.*, **26**, 2310–2323, doi:10.1175/2009JTECHA1281.1.

——, and Coauthors, 2010: The *CALIPSO* mission: A global 3D view of aerosols and clouds. *Bull. Amer. Meteor. Soc.*, **91**, 1211–1229, doi:10.1175/2010BAMS3009.1.

WMO, 1956: *International Cloud Atlas* (abridged). World Meteorological Organization, 62 pp.

Wong, R. K. W., N. Chidambaram, L. Cheng, and M. English, 1988: The sampling variations of hailstone size distributions. *J. Appl. Meteor.*, **27**, 254–260, doi:10.1175/1520-0450(1988)027<0254:TSVOHS>2.0.CO;2.

Wylie, D. P., W. P. Menzel, H. M. Woolf, and K. Strabala, 1994: Four years of global cirrus cloud statistics using HIRS.

J. Climate, **7**, 1972–1986, doi:10.1175/1520-0442(1994)007<1972:FYOGCC>2.0.CO;2.

Yang, P., and K. N. Liou, 1998: Single-scattering properties of complex ice crystals in terrestrial atmosphere. *Contrib. Atmos. Phys.*, **71**, 223–248.

——, and Q. Fu, 2009: Dependence of ice crystal optical properties on particle aspect ratio. *J. Quant. Spectrosc. Radiat. Transfer*, **110**, 1604–1614, doi:10.1016/j.jqsrt.2009.03.004.

——, B.-C. Gao, B. A. Baum, Y. X. Hu, W. J. Wiscombe, M. I. Mishchenko, D. M. Winker, and S. L. Nasiri, 2001: Asymptotic solutions for optical properties of large particles with strong absorption. *Appl. Opt.*, **40**, 1532–1547, doi:10.1364/AO.40.001532.

——, and Coauthors, 2003: Spectral signature of ice clouds in the far-infrared region: Single-scattering calculations and radiative sensitivity study. *J. Geophys. Res.*, **108**, 4569, doi:10.1029/2002JD003291.

——, H. Wei, H.-L. Huang, B. A. Baum, Y. X. Hu, G. W. Kattawar, M. I. Mishchenko, and Q. Fu, 2005: Scattering and absorption property database for nonspherical ice particles in the near-through far-infrared spectral region. *Appl. Opt.*, **44**, 5512–5523, doi:10.1364/AO.44.005512.

——, G. Hong, G. W. Kattawar, P. Minnis, and Y. X. Hu, 2008: Uncertainties associated with the surface texture of ice particles in satellite-based retrieval of cirrus clouds: Part II—Effect of particle surface roughness on retrieved cloud optical thickness and effective particle size. *IEEE Trans. Geosci. Remote Sens.*, **46**, 1948–1957, doi:10.1109/TGRS.2008.916472.

——, K. N. Liou, L. Bi, C. Liu, B. Yi, and B. A. Baum, 2015: On the radiative properties of ice clouds: Light scattering, remote sensing, and radiation parameterization. *Adv. Atmos. Sci.*, **32**, 32–63, doi:10.1007/s00376-014-0011-z.

Zhou, Z. Q., S. P. Xie, X. T. Zheng, Q. Liu, and H. Wang, 2014: Global warming–induced changes in El Niño teleconnections over the North Pacific and North America. *J. Climate*, **27**, 9050–9064, doi:10.1175/JCLI-D-14-00254.1.